UNIVERSITY OF GHANA

COLLEGE OF BASIC AND APPLIED SCIENCES

COMPARISON OF THE PETROLOGY AND MINERAL CHEMISTRY OF THE COROMANDEL AND KIWITAHI VOLCANIC ROCKS, NORTH ISLAND, NEW ZEALAND

MICHAEL MAWULI BOAME

(10277850)

THIS THESIS IS SUBMITTED TO THE UNIVERSITY OF GHANA, LEGON IN PARTIAL FULFILMENT OF THE REQUIREMENT FOR THE AWARD OF MPHIL GEOLOGY DEGREE.

October, 2016.

DECLARATION

This is to certify that this thesis is the result of research undertaken by Boame Mawuli Michael towards the award of Master of Philosophy degree in Geology in the Department of Earth Science, University of Ghana.

…….. Date……

MICHAEL MAWULI BOAME

(MPhil. Candidate)

…….... Date…….

Prof. Prosper M. Nude

(Principal Supervisor)

…….…… Date…….

Prof. Brian Cousens

(Co-Supervisor)

ABSTRACT

This is thesis was done based on the textural, mineralogical and mineral chemistry studies of arc rocks from the North Island of New Zealand. The rocks in the area are of two main groups: the Kiwitahi and Coromandel groups. Both the Coromandel group and Kiwitahi andesites are typically porphyritic with a phenocryst assemblage (20–60%) consisting of plagioclase + pyroxene + Fe –Ti-oxide in a granular groundmass rich in plagioclase laths and pyroxene microcrystals. The Kiwitahi samples consist of andesite, dacite and basalt. The Kiwitahi samples which are from two of the centers namely the Miranda and Tahuna are all andesites. The Coromandel and Kiwitahi rocks are arc rocks and the arc volcanism has migrated south through the North Island over the last 25 Ma. The Colville Ridge is an oceanic arc, and the Coromandel and Kiwitahi are parallel continental arcs, all of which were active during the Miocene. The study was conducted to identify the different rock types in the study area based on their petrology and mineral chemistry and also to determine their state of equilibrium against their state of disequilibrium using the same dataset.

The prepared thin sections were first studied under a petrographic microscope, based on which the petrographic description of the samples was done and photomicrographs of interesting features were taken. Afterwards, selected thin sections were taken to the microprobe laboratory for further studies. The samples were studied under the microprobe and BSE images of interesting features were taken. The Kiwitahi Tahuna andesite was found to be petrologically comparable to the Miranda andesite but lacks hornblende. Plagioclase is the dominant mineral in the samples and occurs as euhedral or subhedral crystals, up to 2-3 mm in size, some of which show complex internal structures. These internal structures which include oscillatory zoning, internal resorption surfaces and sieve textured cores are very common in the plagioclase crystals in the rock, and are indicative of disequilibrium. The pyroxene crystals also have reaction rims with Ti-magnetite inclusions

which is also indicative of disequilibrium. The sieve texture in the plagioclase favours a magmatic interaction process. Thus the samples studied have undergone disequilibrium through magmatic interaction which can possibly be magma mixing due to the occurrence of the sieve and boxy-cellular textures which denotes that the undercooling of a more mafic magma occurred in contact with a cooler more evolved magma.

ACKNOWLEDGEMENT

This work would not have been possible without the support from a number of awesome people. I am grateful to Dr. Brian Cousens for the opportunity to undertake this project, for excellent supervision and for continued support.

Thanks also go to Peter Jones for the probe analysis, BSE images and guidance with data interpretation.

Most importantly, I appreciate Prof. Prosper Nude and Dr. Patrick Sakyi for their advice and support.

Table of Contents

LIST OF FIGURES

CHAPTER ONE

INTRODUCTION

This thesis comprises textural, mineralogical and mineral chemistry study of North Island rocks. The study area is one of the two main islands of New Zealand. The thesis was undertaken to highlight and help understand the similarities and differences between these rocks which are mainly arc rocks. The Colville Ridge is an oceanic arc, and the Coromandel and Kiwitahi are parallel continental arcs, all of which were active during the Miocene. This is why the comparison between Coromandel and Kiwitahi is interesting and of geologic significance.

1.1 BACKGROUND

The Late Cenozoic convergence of the Pacific and Australian plates in the southwestern Pacific region shows a trend over time from basalt and andesite dominated shield and cone volcanism with limited silicic activity in the Northland Arc (Smith et al., 1989), to andesite- and rhyolite-dominated activity in the Coromandel Volcanic Zone (Skinner, 1986), to overwhelmingly silicic volcanism in the Taupo Volcanic Zone (TVZ; Wilson et al., 1995). The 1.8-1.95 Ma, is a volcanically active period in the Coromandel Volcanic Zone a period spanning major tectonic reconfiguration of the SW Pacific region including the waning of volcanism in the Northland Arc (Herzer, 1995; Hayward et al., 2001), the cessation of back arc spreading in the South Fiji Basin (Mortimer et al., 2010) and the inception of back arc spreading in the Havre Trough (Ballance et al., 1999). The rocks of the North Island volcanic succession (Fig 1.1) are mainly preserved on the Coromandel Peninsula and surrounding islands as the Coromandel Volcanic Zone (CVZ). This provides an outstanding

opportunity to study the development of the nascent arc (Booden, 2011). The Kiwitahi chain, which comprises of nine volcanic centers, strikes NNW and was erupted between 15 and 5.5 Ma in New Zealand (Black et al., 1992). Before 6.2 Ma, the erupted rocks were plagioclase- and hornblende -dominated andesites. These are similar to the much larger Coromandel Volcanic Zone (CVZ) (Booden et al., 2010). The petrology and mineral chemistry of the Coromandel and Kiwitahi have been extensively studied (Black, 1957; Black et al., 1992; Booden, 2010; Booden, 2012).

Disequilibrium textures in minerals have been widely observed and studied in igneous rocks (Nixon and Pearce, 1987; Umino and Horio, 1998). They vary and are associated with different disequilibrium types that occur mainly during the evolution of magmatic systems. They are deciphered as the possible effects of varying pressure, temperature and/or composition that perturbed a pre-existing state of equilibrium of the magma body (Dobosi and Fodor, 1992; Rutherford & Hill, 1993; Simonette et al., 1996). Many natural rocks contain clear evidence of disequilibrium, such as compositional zoning and reaction rims because they were formed from magmas crystalizing along non-equilibrium time-dependent pathways. A disequilibrium effect does not propagate homogeneously within a magma volume. This behaviour was described in the study of the coexistence of plagioclase crystals showing very dense zonation patterns that vary markedly from crystal to crystal (Anderson, 1984). Disequilibrium textures have been observed throughout the study area based on the observations made in the sections prepared from the rocks.

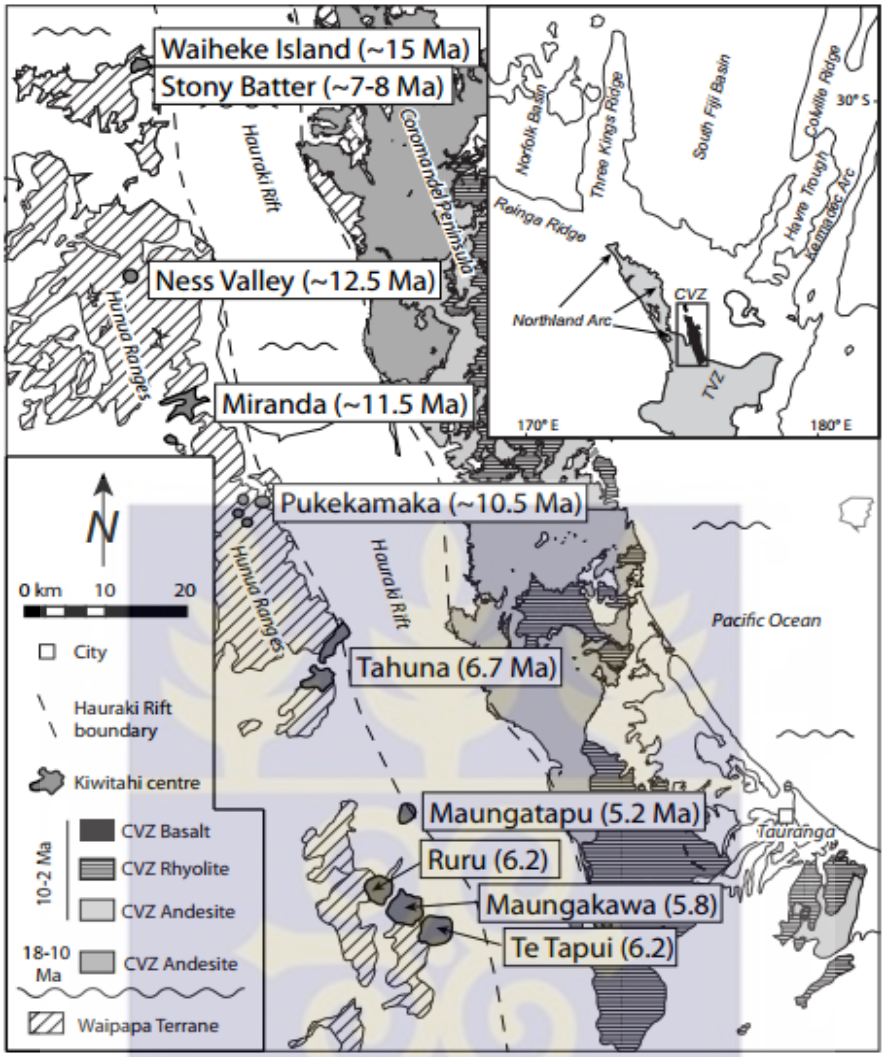

Fig 1.1 North Island Geological map showing geologic units in the study area based on Skinner (1986). CVZ: Coromandel Volcanic Zone. Ages in (Ma) from Black et al. (1992).

1.2 OBJECTIVES

The principal aims of this study are to identify the different rock types in the study area and to determine their state of equilibrium against their state of disequilibrium. This was achieved through the following activities

a. Collection, compilation and interpretation of a high quality petrological and geochemical dataset on a suite of unaltered volcanic rocks that are representative of the Kiwitahi andesite and Coromandel Volcanic Zone rocks.

b. The dataset was used to study the petrology and mineral chemistry of the rocks in the study area

c. The dataset was used to assess and infer the equilibrium against disequilibrium in the rocks.

1.3 STUDY AREA

1.3.1 Location and size

New Zealand, about 1,250 mi (2,012 km) southeast of Australia, consists of two main islands and a number of smaller outlying islands so scattered that they range from the tropical to the Antarctic. New Zealand's two main components are the North Island (Fig. 1.2) and the South Island, separated by the Cook Strait. The North Island (115,777 sq. km), which is the study area is 829 km long and volcanic in its south-central part. It has many hot springs and beautiful geysers. The South Island (151,215 sq. km) has the Southern Alps along its west coast, with Mount Cook (3754 m) the highest point (www. Teara.govt.nz/en/natural-environment/page-1).

1.3.2 Topography and Drainage

The North Island is mainly rolling hill country, much of which is farmed. A series of narrow ranges (Tararua, Ruahine and Kaimanawa) form a roughly north-east belt of higher country that rises up to 1,700 m. Much of the surviving forest cover is found here and in other mountainous areas. In the central North Island, volcanoes that have been active over the past million years jut up thousands of metres near Lake Taupō. This is the country's largest lake, formed by water filling a volcanic crater. Nearby, Rotorua's mud pools boil and geysers erupt. (www. Teara.govt.nz/en/natural-environment/page-1).

Stewart Island is mainly low rolling hills. Unlike the two main islands, it remains almost entirely covered with native vegetation.

1.3.3 Climate

New Zealand is roughly midway between Antarctica and the tropics, lying between 34° and 47° latitude south. The northern outlying islands are subtropical, while those in the south are subantarctic. Between these extremes, New Zealand's climate is cool temperate to warm temperate, but can vary widely, even within one day. It also has microclimates due to its varied topography. The mountain ranges can cause significant climate variations in locations barely tens of kilometres from each other. At New Zealand's location, warm moist air from the tropics meets cold dry air from Antarctica. The two don't mix: they twist around and bump into each other. These swirling air masses sweep over New Zealand from the west (www. Teara.govt.nz/en/natural-environment/page-1).

Large volumes of stable, dry, descending air are known as high-pressure systems, often termed 'highs', which bring settled weather. Eastward-travelling highs cross the country every six to seven days. Between the highs are areas of unstable, ascending air known as low-pressure systems, or 'lows'.

New Zealand's seasons roughly follow this pattern:

Spring arrives in September and October, as the days lengthen and the yellow kōwhai blooms mark the end of colder weather. Springtime is often windy, as variable weather sweeps over the country. Average temperature: 12.1°C. Summer is cool to mild in the south, and mild to warm in the north. Temperatures are normally in the mid to low 20s (°C) over most of the country. It goes up to about 25.5 °C in the North Island. Although Christmas Day is officially in summer, the weather is often still unpredictable. As the days shorten in January and February, there are long fine spells. Average temperature: 16.6°C.

Autumn is the most settled time. In the far north an extended 'Indian summer' is a very real prospect. Average temperature: 13.3°C. Winter is cold, but temperatures are much milder in

New Zealand compared to other areas of similar latitude. Maxima are generally between 10 °C and 15 °C in the North Island, decreasing as one goes further south or inland.

Snow falls in New Zealand, and at higher altitudes in the North Island. It is extremely rare at sea level in the North Island, with one snowfall in both Auckland and Wellington in 2011 after a period of 80 years where none occurred. Snow is more common inland, though snow at sea level does occur on average once or twice per year in the central and southern South Island. Rainfall on the other hand, is generally plentiful, with most cities in North Island receiving between 620 mm and 1317 mm of precipitation annually. The upper part of the North Island, have high humidity all year round, which can have the effect of it feeling warmer in summer and cooler in winter than the thermometer indicates. Rainfall is normally distributed evenly throughout the year in most parts of the country (www. Teara.govt.nz/en/natural-environment/page-1).

1.3.4 Soils and Vegetation

Most New Zealand soils are similar to those elsewhere in the world, but some soils and their properties are unique. New Zealand soils are predominantly acidic. This may be because there is relatively little natural lime present. Native forest species also have an acidifying effect. There are 14 main soil types in the North Island. They are allophanic, brown, brown-stony, grey, granular, melanic, organic, oxidic, pallic, podzol, pumice, raw, recent and ultic soils. Granular and Oxidic soils are limited to the warmer Northland and South Auckland regions, while Allophanic soils and Pumice soils derived from volcanic ash are concentrated in the central North Island. Pallic soils are in the southern districts. (http://www.TeAra.govt.nz/en/soils/page-4)

1.4 GEOLOGICAL SETTING OF THE STUDY AREA

1.4.1 Context of Study

The SW Pacific that includes New Zealand is part of a partly submerged continent that broke away from the Gondwana supercontinent 65 millions of years ago (Herzer et al. 2009). The tectonic history of this area indicates that the convergence of the Pacific and Australasian plates has given rise to multiple episodes of subduction and back-arc spreading (Herzer et al. 2009).

The Pacific plate is being subducted westward under the North Island, but in South Island the boundary is a transform. In North Island, the Taupo Volcanic Zone (TVZ) is associated with contemporary subduction along the Kermadec Trench but the volcanic rocks of the Auckland area and the Northland peninsula are over 400 km from the trench (Huang et al., 1997). Geologically, New Zealand is a juvenile country with most of its oldest rocks not older than the late Paleozoic (Forbes, C., 1855).

Records of volcanism and magmatism in a convergent plate boundary setting are seen in the stratigraphic succession. These are mainly composed of pre-Cenozoic volcaniclastics and plutonic rocks of the basement terranes and Cenozoic volcanic cover sequence rocks. (Booden et al., 2010). Subduction volcanism was predominant in the Coromandel Volcanic Zone (CVZ), an area in the Northwestern North Island comprising the Coromandel Peninsula, Great Barrier Island and surrounding Islands, from the Middle Miocene to the Quaternary.

The Kiwitahi chain, which consist of nine volcanic centers, strikes NNW and was erupted between 15 and 5.5 Ma in New Zealand (Black et al., 1992). Before 6.2 Ma, the erupted rocks were plagioclase- and hornblende -dominated andesites. These were similar to the much larger Coromandel Volcanic Zone (Booden et al., 2010).

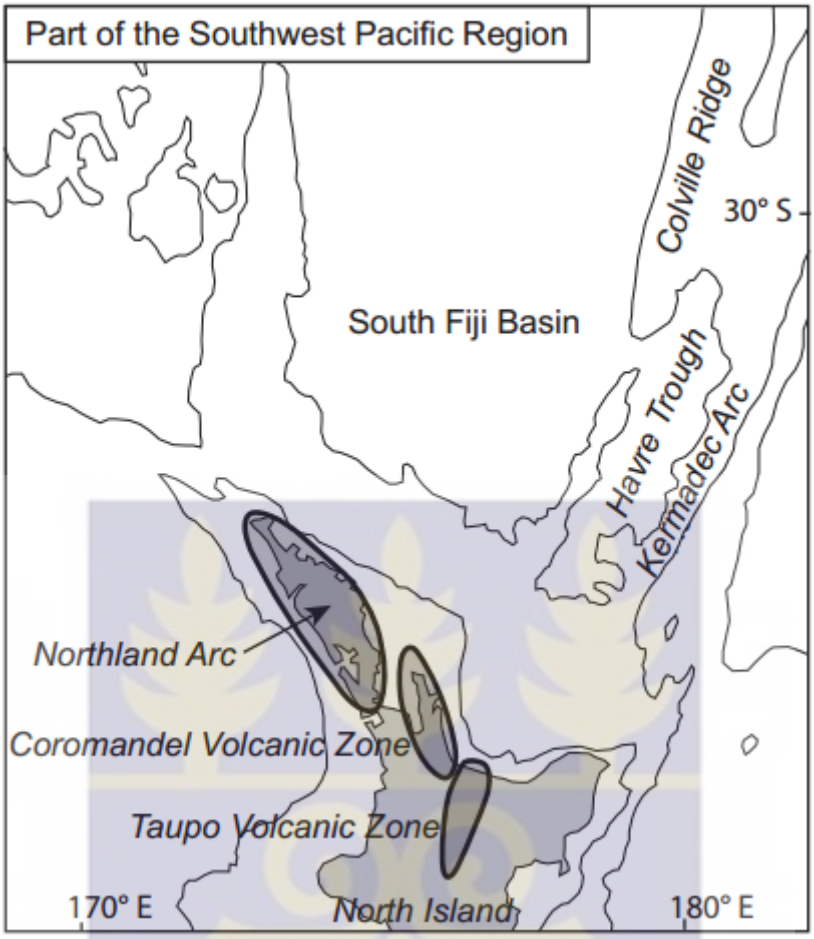

Fig 1.2: Major tectonic features of the SW Pacific region and major volcanic zones of the North Island of New Zealand.

The intermittent volcanism in the Kiwitahi chain developed concurrently with approximately continuous volcanism in the Coromandel Volcanic Zone. Several features suggest that the Kiwitahi centers represent the continental edge of the CVZ magmatic system:

(a) the older Kiwitahi centers, from NE Waiheke Island to Tahuna, are incrementally younger to the SSE, mirroring the migration of the volcanic front in the CVZ; (Booden et al., 2010).

(b) the pre-10 Ma Kiwitahi centers erupted amphibole-bearing andesite, whereas the younger centers did not, which is a trend also observed in the CVZ andesites; (Booden et al., 2010).

(c) prior to ~7 Ma, the Hauraki Rift did not exist as a tectonic divide between the basement highs of the Coromandel Peninsula and the Hunua Ranges (Hochstein and Ballance 1993).

The key trace element difference between Kiwitahi andesites and coeval CVZ andesites with comparable major element compositions is the lesser incompatible element enrichment in the Kiwitahi rocks. This could argue for either a greater degree of partial melting in the source of the Kiwitahi andesites, or for lesser assimilation of low-degree, differentiated partial melts by Kiwitahi andesites (Booden, 2011). Because the low incompatible element enrichment correlates with relatively low initial $^{87}Sr/^{86}Sr$ ratios in Kiwitahi rocks with the exception of Tahuna, this occurrence can best be explained as a lesser interaction with differential crustal partial melts in the petrogenesis of the Kiwitahi magmas (Booden, 2010).

The generation of Kiwitahi magmas is perceived as occurring on the edge of a "hot zone" near the crust-mantle interface, which is the energetic and central most part of which it was located at any given instant in time underneath the CVZ. It is speculated that, on the edge of the hot zone, a less energetic environment existed where crustal anatexis was suppressed and magmas did not readily absorb a substantial crustal component. The smaller magma volumes that were presumably involved are consistent with less frequent eruptions and more mafic magma compositions (typically <60% SiO_2), relative to the CVZ. This regime gave rise to the eruptions at the Waiheke-Pukekamaka and Tahuna centers.

CHAPTER TWO

LITERATURE REVIEW

2.1 ZEALANDIA

New Zealand is the emergent part of a larger continental fragment that is about one third the area of Australia (Mortimer, 2004). The basement rocks of this 'Zealandia' (Luyendyk, 1995) are exposed on New Zealand and the surrounding islands. They form a series of terranes that comprise Palaeozoic and pre-110 Ma Mesozoic, variably metamorphosed and deformed sedimentary, volcanic and plutonic rocks. The terranes generally strike N-S and are inferred to have formed at, or accreted to, the convergent margin of eastern Gondwana. The break-up of the supercontinent is recorded in Zealandia by the development of half-grabens and metamorphic core complexes between 110-85 Ma, representing the rifting of Zealandia from Gondwana (Spell et al., 2000) and the subsequent opening of the Tasman Sea and Fairway-Aotea basins to the west and of the Southern Ocean to the south (Gaina et al., 1998). In the Gondwana jigsaw puzzle, Zealandia restores to a position SE of Tasmania, Australia (Sutherland, 1999), and North of Marie Byrd Land, Antarctica (Stock and Candle, 2002).

2.2 THE SOUTHWEST PACIFIC REGION

Zealandia straddles the N- to NNE-striking Australian-Pacific convergent plate boundary, where the Cretaceous Pacific plate (Watts et al., 1988) subducts in western direction underneath the Australasian plate, giving rise to subduction-related volcanism on the Australasian plate that forms the c. 2500 km long Tonga-Kermadec arc (Smith and Price, 2006). This arc is contiguous with the Taupo Volcanic Zone in the central North Island. North and northeast of Zealandia, behind-arc from the convergent plate boundary, lies the

SW Pacific region, which is characterised by a complex of generally North-trending continental ribbons, spreading centres and volcanic arcs, the origin and evolution of which has been the subject of recent debate (Herzer et al., 2000; Crawford et al., 2003; Schellart et al., 2006; Whattam et al., 2006; Mortimer et al., 2007; Schellart, 2007; Whattam et al., 2008; Herzer et al., 2009; Mortimer et al., 2010).

The spreading centres generally become older farther west from the present plate boundary. Directly behind, i.e. to the west of, the Kermadec Arc lays the Havre Trough backarc basin, a region of nascent, disorganised seafloor spreading since approximately 5.5 Ma (Ballance et al., 1999; Wysoczanski et al., 2010).

To the north, the Havre Trough is contiguous with the Lau backarc basin. The rates of convergence along the plate boundary, as well as the rates of extension in the back-arc basins, increase in a northward direction, from 42 and 8 mm yr^{-1} (Darby et al., 2000), respectively, at the North Island segment, to 53 and 15 mm yr^{-1} at 35°S, to 85 and 159 mm yr^{-1} at 16°S near the northern termination of the arc (DeMets et al., 1994). To the west, the Havre Trough backarc basin is bounded by the NNE-striking Colville Ridge. This is essentially the extinct western part of what is now the Kermadec Arc (Balance et al., 1999). 40Ar/39Ar dating of dredged basalt from the Colville Ridge indicates that it was an active volcanic arc at least as early as 16.7 Ma (Mortimer et al., 2010).

The Colville Ridge and the Kermadec each have sharply defied boundaries with the intervening Havre Trough backarc basin, characterised by c. 2.5 km scarp faces on both sides. Within the Havre Trough basin, the thickest sediment accumulation occurs on the western side (Ballance et al., 1999).

Volcanic edifies occur within the basin along lineaments that strike perpendicular to the arc and are aligned with some Kermadec Arc volcanoes. These trails have been interpreted as recording migrating arc volcanism in response to trench-ward retreat of the volcanic front

(Wright et al., 1996). To the west of the Colville Ridge consecutively occur the 1200 km wide South Fiji Basin spreading center, the Three Kings Ridge, the Norfolk basin and the Norfolk Ridge.

South Fiji and Norfolk basin MORB and back-arc basin basalts have been dated by 40Ar/39Ar method at Late Oligocene to Early Miocene (26-18 Ma) (Mortimer et al., 1998) although magnetic anomaly data also suggest that parts of the Norfolk Basin may be Cretaceous (Davey, 1982; Malahoff et al., 1982).

The Norfolk basin experienced extensional tectonics from c. 34 Ma (DiCaprio et al., 2009). The Norfolk Ridge is a continental ribbon that comprises Mesozoic basement crust (Mortimer et al., 1998). The Norfolk and Three Kings ridges were each the site of Early Miocene (32-26 Ma) subduction- and rift-related volcanism (Mortimer et al., 2007).

The SW Pacific volcanic ridges and backarc basins are separated from the Mesozoic crust of Zealandia by the NW-striking Vening Meinesz Fracture Zone (VMFZ). Between the South Fiji Basin and Zealandia, the Northland Plateau additionally occurs north of the VMFZ. It comprises c. 12-16 km thick crust and is divided into a sedimentary inner plateau on the continental side and a volcanic outer plateau, which is geophysically contiguous with the Three Kings ridge (Herzer et al., 2000; Herzer et al., 2009).

2.3 THE NORTH ISLAND VOLCANIC SUCCESSION

Cenozoic subduction-related volcanic rocks in northern New Zealand principally occur in a belt stretching from Northland, via the Coromandel region to the central North Island. Submerged and buried subduction-related volcanic rocks further occur offshore west of the Northland, Waikato and Taranaki regions, and several volcanic centres formed in a behind-arc setting in the western North Island. The succession has been geographically divided into three major volcanic zones: the Northland Arc, which comprises Late Oligocene to Middle

Miocene volcanic centres in Northland and the offshore Northland Basin; the Coromandel Volcanic Zone, which comprises Middle Miocene to Pleistocene volcanic centres in the Coromandel peninsula, on Great Barrier Island and in the wider Hauraki region; and the Taupo Volcanic Zone, which comprises Pleistocene-Recent volcanic centres in the central North Island and the Bay of Plenty (Booden et al., 2010).

2.3.1 Northland arc

The remnants of Late Oligocene to Middle Miocene subduction-related volcanism are preserved on the NW-trending Northland Peninsula, which extends from the North Island and is contiguous with the submerged Reinga Ridge. It is bounded in the west by the Cretaceous-Paleogene Northland Graben (Uruski et al., 2004). To the north, the continental shelf extends to the Vening Meinesz Fracture Zone. The basement comprises deformed Permian to Jurassic metasedimentary and igneous rocks of the Murihiku, Maitai and Waipapa basement terranes (Sivell and McCulloch, 2000; Adams and Maas, 2004; Mortimer, 2004). The smaller Mt. Camel Terrane comprises a distinct Late Cretaceous sequence of clastic sediments and keratophyric volcanic rocks (Nicholson and Black, 2004). Early Tertiary sedimentary rocks locally unconformably overlie the basement rocks. Nappes of the Northland Allochthon comprising allochthonous Cretaceous to Paleogene igneous and sedimentary rocks in turn overlie the basement and its autochthonous cover. These nappes were thrust onto Northland in southeastern and southwestern direction during the Oligocene and Miocene and have total stratigraphic thickness of c. 7 km (Ballance and Spörli, 1979).

Rootless ophiolite massifs occur in the uppermost nappe (Sharp et al., 1989; Malpas et al., 1992). They comprise minor Cretaceous oceanic crust, but mostly Oligocene oceanic crust with a subdued arc-type trace element signature, which has been inferred to represent

oceanic lithosphere formed in a fore-arc spreading center over a NE-dipping subduction zone north of New Zealand. Additionally, minor 25-15 Ma boninitic, alkalic and calc-alkaline rocks occur that possibly represent fore-arc correlatives to the developing Northland Arc (Whattam et al., 2004; Whattam et al., 2006).

2.3.2 Northland arc - volcanism

From the Late Oligocene to the early Middle Miocene, two parallel volcanic belts separated by 30- 60 km formed in Northland (Ballance, 1976; Kear, 1994). The belts were simultaneously active and do not show an unequivocal trend in the distribution of individual centers' ages, other than that the oldest rocks are preserved in the northernmost center (~25.5 Ma, North Cape) and that volcanism persisted longest in the south (~15.5 Ma, Manukau/Waitakere center; Fig. 2.2) (Hayward et al., 2001).

The known Northland Arc is unusually non-linear, being approximately 200 km wide (NE to SW) and 350 km long, striking NW. However, a dredged basaltic andesite from the Reinga Ridge, 40Ar/39Ar dated at 21.0 Ma, could represent the northwestern most known Northland Arc activity, and if so the total length of the arc is at least 500 km (Mortimer et al., 2010). Northland Arc rocks generally have an arc-type trace element composition.

Additionally, a distinct style of volcanism is recorded by polymict, partly volcaniclastics conglomerates in the Waitemata Basin containing 20 Ma basaltic pebbles with an ocean island basalt (OIB)-like trace element distribution.

They have been interpreted to represent asthenosphere-derived magmas that erupted where mantle upwelling occurred around the slab edge (Shane et al., 2010, and references therein). Four western belt volcanic centers are preserved onshore. The Waipoua center is the remnant of a basaltic shield volcano, and the Manukau/Waitakere center is the remnant of a basaltic andesitic cone complex (Smith et al., 1989). The remains of both of these centers

still form topographic highs onshore and can be traced on seismic sections up to 30-50 km west of the present coastline (Herzer, 1995). The Hukatere and Tokatoka centers have a much smaller aerial extent, occur entirely on-land, and comprise dispersed plugs, dykes, flows and pyroclastic sequences (Smith et al., 1989). Additionally, six larger, and numerous smaller volcanic centers have been identified on seismic sections off the west coast of Northland.

The maximum ascertainable ages of the oldest centers are around 22 Ma, although the remains of earlier volcanism may be masked by younger rocks. Volcanism in the offshore western belt declined from ~19 Ma and had ceased entirely by 16 Ma (Herzer, 1995). Western belt rocks are typically strongly porphyritic plagioclase + pyroxene ± olivine phyric basalts, basaltic andesites and andesites; dacites and rhyolites are rare (Smith et al., 1989).

The eastern belt comprises three major volcanic and sub-volcanic centers that are preserved partly onshore along the east coast of Northland. The predominant rock types in this eastern belt are two-pyroxene andesites, hornblende andesite and hornblende dacites, with subordinate rhyolite and basaltic andesite (Smith et al., 1989). Some andesite lavas at the Taurikura center contain grossular-rich garnet (Day et al., 1992). In contrast to the western belt, basalts are nearly absent (Smith et al., 1989).

2.3.3 Coromandel volcanic zone

The Coromandel Volcanic Zone (CVZ) comprises volcanic rocks on Great Barrier Island, the Coromandel Peninsula and surrounding islands. The wider 'Hauraki Volcanic Region' further includes small volcanic centers of the Kiwitahi volcanic chain (Skinner, 1986). The Miocene-Pliocene CVZ succession erupted to the SE of the older Northland Arc eastern

belt, and is on lapped in its southeastern segment by deposits of the younger Taupo Volcanic Zone (TVZ).

Mesozoic meta-sedimentary basement rocks of the Waipapa Terrane are exposed in the northern Coromandel peninsula and on Great Barrier Island (Skinner, 1972). At localities in the northern Coromandel peninsula and on Great Barrier Island, Waipapa Terrane rocks have whole-rock K-Ar ages between 142.7 ± 2.8 and 101.4 ± 2.0 Ma (Adams and Maas, 2004). The basement is locally unconformably overlain by Early Cenozoic sediments (Skinner, 1986).

The NNW-trending Coromandel peninsula is a horst that follows basement fault trends, and is flanked by the Hauraki Rift, a half-graben that is downthrown to the east (Hochstein et al., 1986; Hochstein and Ballance, 1993). The timing of the initiation of subsidence in the Hauraki Rift is ambiguous. Hochstein and Ballance (1993) suggested a possible Late Miocene inception at c. 7 Ma.

Hayward et al. (2006) proposed possible initiation in the early Pleistocene, based on the occurrence of quartz vein and altered andesite pebbles with a likely provenance in the Coromandel peninsula in Pleistocene conglomerates west of the Hauraki Rift.

Briggs et al. (2005) demonstrated that in its southern segment, at least 40% of throw on the Hauraki Fault occurred between 2.09 and 1.21 Ma. Each of these interpretations has subsidence post-dating most CVZ volcanism.

2.3.4 Coromandel volcanic zone – volcanism

The CVZ volcanic succession covers much of Great Barrier Island, the Coromandel Peninsula and the wider Hauraki region. As well, submerged igneous rocks form a plateau that extends towards the Colville Ridge (Skinner, 1986). The oldest, 18Ma volcanic rocks occur in the northern Coromandel Peninsula, the youngest c. 2Ma rocks occur in the

southernmost CVZ; Adams et al., 1994a; Brathwaite and Christie, 1996; Briggs et al., 2005). The same age trend occurs in the SSE-striking Kiwitahi chain, a series of small volcanic centres that formed along the western boundary of the Hauraki Rift (Black et al., 1992).

Volcanic rocks in the CVZ form four main rock types: basalts, high-magnesium andesites, calc-alkaline andesites and rhyolites. Calc-alkaline andesites and rhyolites form approximately 60% and 40% of the volcanic cover, respectively (Christie et al., 2007), whereas high-magnesium andesites and basalts erupted in subordinate volumes at the continental and oceanic margins of the CVZ.

2.3.4.1 Coromandel group

Early volcanism in the CVZ, between 18-12 Ma, consisted only of basaltic andesitic, andesitic and dacitic cone-building eruptions in the northern Coromandel peninsula, on Great Barrier Island and in the northern Kiwitahi chain (Black et al., 1992; Adams et al., 1994a). Between 12 and 2.5 Ma, the same style of andesitic volcanism persisted in addition to the progressive appearance of rhyolites and basalts (c. 12 Ma) and high-magnesium andesites (c. 6.2 Ma).

This andesitic succession forms the Coromandel Group and occurs as massive flows, autoclastic breccias, lahars, tuffs and dykes (Skinner, 1986). As well, uplifted basement rocks host shallowly intruded, subvolcanic plutons at Paritu in the northern Coromandel peninsula, at Miner's Head on Great Barrier Island and on Cuvier Island in the northern CVZ (Skinner, 1972). The plutons comprise gabbro, diorite, granodiorite and tonalite with ages in the range 17.6-16.4 Ma (Richards et al., 1966; Adams et al., 1994a; Adams et al., 1994b). The Coromandel Group succession is subdivided into four subgroups, each comprising a number of formations distinguished on the basis of petrographic properties and field relations (Skinner, 1986).

The volcanic and subvolcanic Coromandel Group rocks in the northern CVZ form the Kuaotunu Subgroup. Coromandel Group rocks in the central CVZ with ages between 10 and 5.5 Ma form the Waiwawa and Omahine Subgroups, which are distinguished on a stratigraphic basis: Waiwawa Subgroup andesites occur at a lower stratigraphic level than Whitianga Group rhyolites, whereas the Omahine Subgroup comprises andesites that overlie the rhyolitic succession of the Whitianga Group.

The Kaimai Subgroup comprises the andesitic rocks in the southern CVZ. The relative chronology was validated by radiometric dating (Adams et al., 1994a; Brathwaite and Christie, 1996; Briggs et al., 2005): Kuaotunu Subgroup rocks erupted prior to 10.5 Ma; the Waiwawa and Omahine Subgroups have mostly overlapping ages between 10-5.5 Ma, although locally Omahine Subgroup rocks postdate Waiwawa Subgroup rocks; and Kaimai Subgroup rocks, including the andesitic rocks of the southernmost CVZ, have ages younger than 6 Ma.

2.3.4.2 Whitianga Group

Rhyolites in the CVZ form the Whitianga Group and occur on Great Barrier Island, on Great Mercury Island and the Aldermen Islands east of the Coromandel Peninsula, and on the eastern half of the peninsula itself. Whitianga Group includes the eruptive silicic rocks that are preserved on the Coromandel Peninsula, Great Barrier Island, and the Aldermen and Mercury Islands. Whitianga Group rhyolites principally occur as lavas and as ignimbrite sheets, related to 12 Ma volcanic centres, of which at least some were calderas (Briggs and Fulton, 1990; Skinner, 1993; Skinner, 1995; Brathwaite and Christie, 1996; Briggs et al., 1996; Malengreau et al., 2000; Smith et al., 2006a).

The earliest silicic activity is recorded on Great Barrier Island and nearby Rakitu Island, dated at c. 11.5 Ma (Nicholson et al., 2004). Silicic activity continued in offshore centers and recommenced on Great Barrier Island between 8.8-8.1 Ma (Nicholson et al., 2004). On

the Coromandel Peninsula, the oldest recorded silicic eruption formed the Carina Rock Ignimbrite (10 Ma); major silicic activity associated with caldera formation on the Coromandel Peninsula is recorded from 8.1 Ma (Adams et al., 1994a). Rhyolitic eruptions in the CVZ continued at least until 1.95 Ma in the Tauranga area (Adams et al., 1994a,b; Briggs et al., 2005). Although the onshore record shows hiatuses, fission-track ages of silicic tephras recovered by ocean drilling in the Pacific east of the CVZ show a mostly continuous record of eruptions from c. 12 Ma to the end of CVZ activity. However, a significant, c. 700 Ma hiatus with no recorded silicic eruptions occurred between 7.0 and 6.3 Ma (Carter et al., 2003).

Three subgroups of the Whitianga Group are identified by Skinner (1986) and Brathwaite and Christie (1996), each comprising a number of formations. The Coroglen and Ohinemuri subgroups comprise ignimbrites, some of which record caldera-forming eruptions, as well as diverse intercalated rocks. The Minden Rhyolite Subgroup includes rhyolitic lavas that occur mainly as domes.

About eight calderas have been identified, with diameters in the order of 15 to 20 km based on field mapping and geophysical data (Skinner, 1986; Malengreau et al., 2000; Smith et al., 2006a). The calderas are characterised by regional gravity field lows, contrasting with the neutral or positive anomalies associated with intermediate volcanics of Coromandel Group. Gravity data modelling indicates the Kapowai, Whitianga and Wharekawa calderas in the northern and central CVZ are filled with rhyolitic material to depths of 1.5-1.8 km below sea level (Malengreau et al., 2000).

The Waihi Caldera in the southern CVZ comprises silicic material to a depth of close to 3 km, and has been identified as a trapdoor caldera that follows pre-existing fault patterns (Smith et al., 2006a).

2.3.4.3 Mercury Basalts

Basalts and basaltic andesites that erupted in the Mercury Islands, Aldermen Islands and on the eastern sides of Great Barrier Island and the Coromandel Peninsula form the mercury basalts. They are preserved as the remnants of small volcanoes, some of which formed through strombolian type eruptions producing ash and bombs, but more commonly most centres formed through Hawaiian-type sheet flows with a central spatter cone. Mercury Basalts are also preserved as dikes, commonly intruding rhyolite (Skinner, 1976; Skinner, 1986).

The oldest preserved Mercury Basalts occur on Rakitu Island near Great Barrier Island and have been dated at c. 12.1 Ma, pene-contemporaneous with rhyolitic volcanism in the same location (Nicholson et al., 2004). Subsequent basalt eruptions occurred on the Coromandel Peninsula between 9.1 and 7.8 Ma, on the Mercury Islands and at Woody Hill on the peninsula between 6.0-4.6 Ma, and on Matakana Island at 2.7 Ma (Adams et al., 1994a; Briggs et al., 2005). Basaltic rocks that form the Sugarloaf rocks north of the Aldermen Islands are undated. Otherwise, the rocks on Kuaotunu Peninsula are generally more primitive than those of the Mercury Islands (Adams et al., 1994a), indicating a trend to more evolved compositions with time.

2.3.4.4 Kiwitahi Volcanics

A chain of volcanic centres, the Kiwitahi Volcanics, occurs along the western boundary of the Hauraki Rift. They are included in the Coromandel Group (Skinner, 1986). The centres are typically very small and poorly preserved, commonly as fields of massive boulders that probably represent remnants of lava flows. Only the southernmost, youngest centres preserve volcanic cone morphology. The Kiwitahi centres generally become younger to the south. The four oldest centres erupted between c. 15 Ma and 10.5 Ma (Black et al., 1992)

and comprise hornblende-phyric andesite comparable to the andesites of the Kuaotunu Subgroup.

The younger Tahuna centre erupted at 6.7 Ma (Black et al., 1992) and comprises hornblende-absent andesite, comparable to the andesite of roughly contemporanous formations of the Waiwawa Subgroup (Brathwaite and Christie, 1996). Between 6.2-5.5 Ma, clinopyroxene-dominated basaltic andesites erupted in four centres at the southern end of the chain. These rocks do not directly resemble coeval andesites in the CVZ.

Additionally, olivine-phyric basaltic andesite erupted at c. 8 Ma from a vent in close geographic association with the oldest, c. 15 Ma centre at Stony Batter on Waiheke Island (Black et al., 1992). The Stony Batter basaltic andesites compositionally resemble slightly older rocks that erupted at Ti Point in Northland, and have been interpreted as part of a back arc volcanic suite (Black et al., 1992; Smith et al., 1993; Smith et al., 1995; Huang et al., 2000).

CHAPTER THREE

METHODOLOGY

3.1 SAMPLE SELECTION

The samples analysed in this study are part of Professor Brian Cousens' personal rock collection at the Department of Earth Sciences, Carleton University. Twenty-five samples were selected from the collection. The philosophy in the sample selection is as follows:

a) More prominent formations, in terms of aerial extent or stratigraphic thickness, were represented by a relatively larger number of samples.
b) Samples selected from a particular formation were compositionally representative of that formation.
c) Only fresh unaltered samples were selected
d) Samples were selected in order to attain an approximate representative section through the volcanic stratigraphy of the Northland and Coromandel volcanic zone.

3.2 ANALYTICAL WORK

The analytical work stage of the research included thin-section preparation, petrographic studies/analyses, and preparation of samples for electron microprobe analysis.

3.2.1 Thin section preparation

Thin-section preparation, petrographical analysis and EPMA were carried out at the Department of Earth Sciences Honors Laboratory, Carleton University.

The rock samples were cut into smaller rectangular blocks (billets) with a diamond bladed rock saw. Surfaces of the rectangular blocks were ground flat and smoothened using silicon carbide powder. The smoothened surfaces of the blocks were mounted on glass slides using

Canada balsam. The other surfaces were polished and ground down with silicon carbide powder grade 80 until the rocks became thinner. Finer abrasives were progressively used as the section became much thinner. Six hundred (600) silicon carbide powder was used at the later stage of grounding until the thicknesses of the rocks were about 30 microns.

Continuous observation of interference colours of minerals like feldspar and quartz under the petrographic microscope helped in gauging the thicknesses of the sections. The sections were then covered with a glass cover-slip cemented with Canada balsam after carefully clearing and scraping away excess cement.

3.2.2 Petrographical analyses

Out of the several samples, twenty-five (25) prepared thin sections were studied with a petrographic/polarized microscope. This was done to help in identifying the minerals and microstructures to support the mesoscopic observations made on the field. The sections were studied both in plane light and crossed polarised light.

Quantitative description of the thin section incorporated modal analysis, and textural analysis (including grain size, shapes, orientation and inclusions of mineral grains, mineral overgrowth and intergrowth textures as well as their associations).

Photomicrographs were taken of each thin section examined using the ProgRes software and its camera which was fitted to a microscope and a computer. The appropriate rock names were given to the different rocks encountered in the field after careful mesoscopic (hand specimen) observation and modal analysis of the rocks.

Representative rock thin sections were selected for petrographic and geochemical analysis.

3.3.3 Mineral chemistry

The electron microprobe was also used to analyse some of the samples in order to determine the mineral chemistry of the rocks, by doing a qualitative mineral identification and quantitative analyses of the individual minerals. It was also used to take Digital Back-Scattered images and also to help determine state of equilibrium against the state of disequilibrium within.

3.3.3.1 Samples Preparation for mineral Chemistry

Thirteen (13) of the thin sections were resampled from the 25 used for the petrographic analysis for the chemical analysis, which was done at the Earth Sciences department of Carleton University. The thin section to be used for the mineral chemistry was initially carbon coated to protect the surface and the minerals to be analyzed were marked out.

3.3.3.2 Analytical Technique

Using a Cameca Camebax Electron probe equipped with 4 WDX spectrometers, a Henderson automation system, a Kevex EDX x-ray detector, an Aptec model FP6300B spectroscopy amplifier and a Liquid nitrogen sensor. Quantitative analyses were made on an automated 4 spectrometer Camebax MBX electron probe by the wavelength dispersive x-ray analysis method (WDX).Qualitative mineral identifications were made with an energy-dispersive x-ray analysis system (EDX). Operating conditions were: 20 kv accelerating potential and a beam current of 20 nano-amperes (nA) for silicates. Beam sensitive minerals such as feldspar were analyzed using a rastered electron beam 5x5 to 10x10 microns in size. Peak counting times for analyzed elements were: 15-40 seconds or 40,000 accumulated counts. Background positions were chosen carefully to avoid interferences from adjacent peaks. Background measurements were made at 50 % peak counting time on

each side of the analyzed peak. Raw x-ray data were converted to elemental weight percent by the Cameca PAP matrix correction program. A suite of well characterized natural and synthetic minerals and compounds were used as calibration standards.

Digital Back-Scattered Electron (BSE) images were collected with an Electron Optic Services digital imaging system at 512 x 512 pixel resolution with a Lamont 4 element solid state BSE detector and BSE Quad Summing Amplifier interfaced to: a 4Pi Analysis Inc. digital imaging and EDX x-ray system and Power Macintosh computer running NIH image and NIST desktop spectrum analyzer programs.

3.3.3.3 Data Analyses

The dataset obtained from the field and laboratory work have been compiled into tables, maps, graphs and diagrams. The data was processed with computer software including ArcGIS, Microsoft Excel 2010 and ProgRes.

The ArcGIS was used to digitize the geological map and plot the sample points. the graphs and tables were put together using Microsoft excel 2010 and the photomicrographs were snapped and organised with the ProgRes software.

CHAPTER FOUR

RESULTS

This chapter presents the various results gathered from the petrographic analysis and Electron Probe Micro-Analysis. It has been grouped into petrography and mineral chemistry respectively.

4.1 FIELD RELATIONS

The map with sample locations of all the various rocks is shown below in Fig 4.1. The rocks in the study area are mainly Arc rocks characterised by the presence or absence of Amphibole. The study area is divided into two the eastern side which is the Coromandel and the western side, which is the Kiwitahi. The Kiwitahi which consists of nine centers had two of its centers sampled for this study. One of the samples came from the Kiwitahi Miranda center and the other from the Kiwitahi Miranda center.

From the petrographic study, the Coromandel rocks consist of andesites, dacite and basalts. The andesites have been divided into five types namely: the plagioclase- pyroxene andesite, plagioclase- hornblende andesite, hornblende- plagioclase andesite, hornblende- pyroxene andesite and hornblende-pyroxene- plagioclase andesite (Fig 4.1).

The Kiwitahi was found to consist of andesites; which mainly differed by the presence or absence of Amphiboles. The Miranda Andesites are mainly hornblende-pyroxene-plagioclase andesite while the Tahuna andesites are mainly plagioclase-pyroxene andesite. Andesites from three localities were studied, the Coromandel and samples from the Kiwitahi Chain, specifically from the Kiwitahi Tahuna and Kiwitahi Miranda.

They are typically porphyritic-aphanitic with a few trachytic textured samples, and an estimated phenocryst assemblage of (20-55%), which is made up of mainly plagioclase + pyroxene + amphibole.

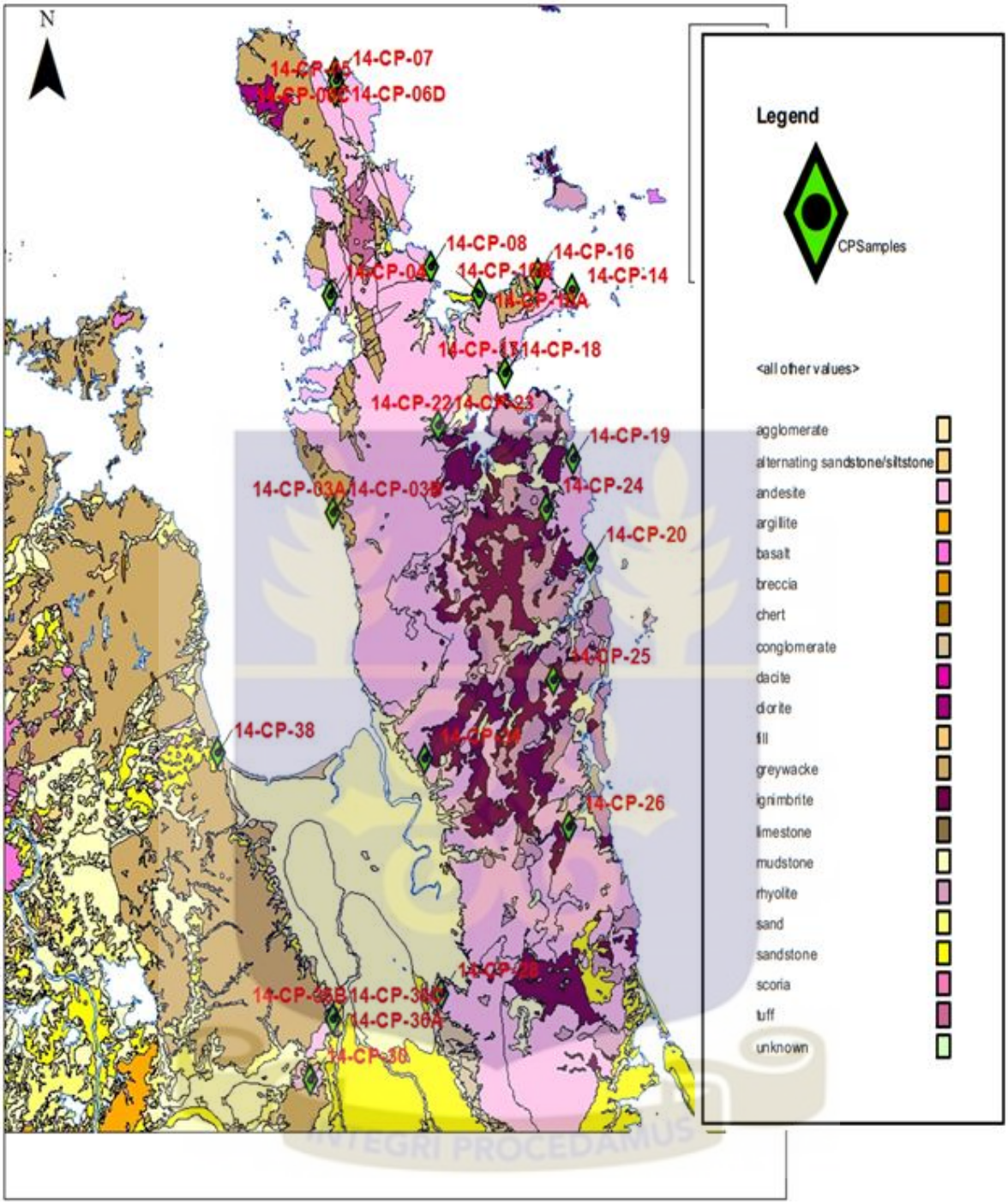

Fig 4.1: Geological Map of the study area showing sample points

The Kiwitahi andesites have a porphyritic–aphanitic texture. The Phenocryst assemblage based on estimation makes, up 20-60% of the sample consists mainly of plagioclase + pyroxene with plagioclase occurring as microlite in the matrix, it is considered the most abundant phase. Olivine is also present in some of the samples.

The Miranda andesites are mainly hornblende-pyroxene–plagioclase andesite and the Tahuna andesites are plagioclase pyroxene andesites.

4.2 PETROGRAPHY

Twenty-five (25) polished sections were studied under the microscope. They were mainly volcanism produced andesites, basalts and dacites from the northern Coromandel and northern Kiwitahi.

The Coromandel andesites have granular groundmass concentrated with plagioclase lath and pyroxene microlite. Plagioclase (20-30% vol.) is the most abundant phenocryst followed by pyroxenes (10-25% vol.), amphibole (1-3% vol.), Ti-magnetite (1% vol.) and olivine (0.5% vol.). Plagioclase is the most common mineral in both the phenocryst and matrix of all the samples. The phenocryst is euhedral to anhedral in form with crystals measuring up to 2-4mm in size.

Almost all the plagioclase crystals show oscillatory zoning (Fig. 4.2) and albite twinning or both albite and pericline twinning. The zoning varied from simple oscillatory to complex patchy types. Most of the crystals have inclusions and lamellae consisting of pyroxenes. Most of the samples contain ubiquitous sieve texture in the core of the plagioclase crystals (Fig. 4.2), the sieve texture is observed to be replacing the older oscillatory growth zones.

Most feldspar crystals with the sieve texture have clear growth rims (Fig. 4.2). Internal resorption or embayed surfaces that are lacking in inclusion also occur (Fig. 4.3). The inclusions within the plagioclase are mainly pyroxenes. There is the occurrence of cumulophyric cluster of plagioclase and pyroxenes phenocryst. The second most abundant phenocryst is pyroxene, the crystal are euhedral to subhedral. It consists mainly of clinopyroxenes and orthopyroxenes. The crystals are spread out evenly throughout the

samples. There is also the occurrence of pyroxene crystals with coronas (Fig 4.3), these coronas also show zoning. Most of the rims are made of clinopyroxene with Ti-magnetite inclusions (Fig 4.3). The rims measure to about 50 microns thicks. There is also the occurrence of clinopyroxene lamellae in some of the orthopyroxene crystals

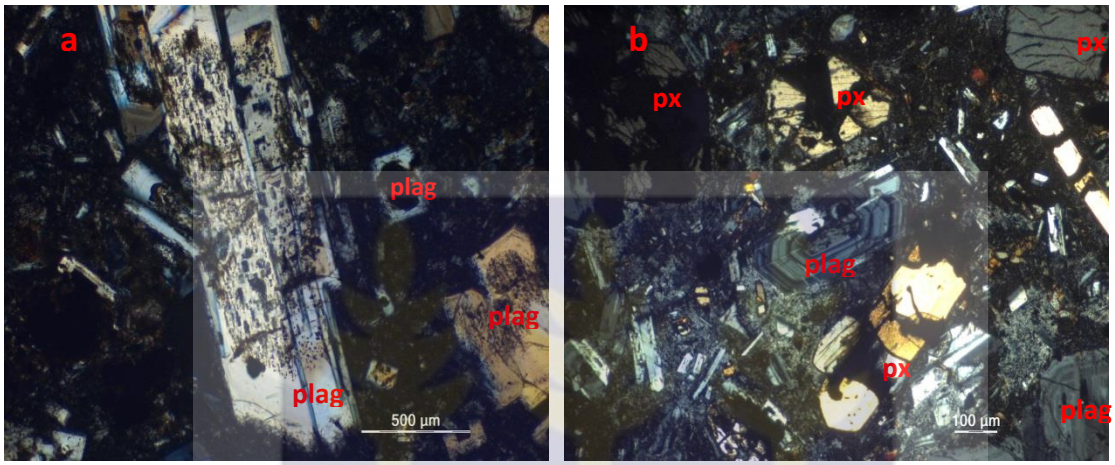

Fig. 4.2 Photomicrograph of Coromandel Andesite (a) a plagioclase (plag) crystal with an sieve-textured core and clear rims (XPL). (b) plagioclase (plag) with concentric zoning and pyroxene (px) inclusion (XPL).

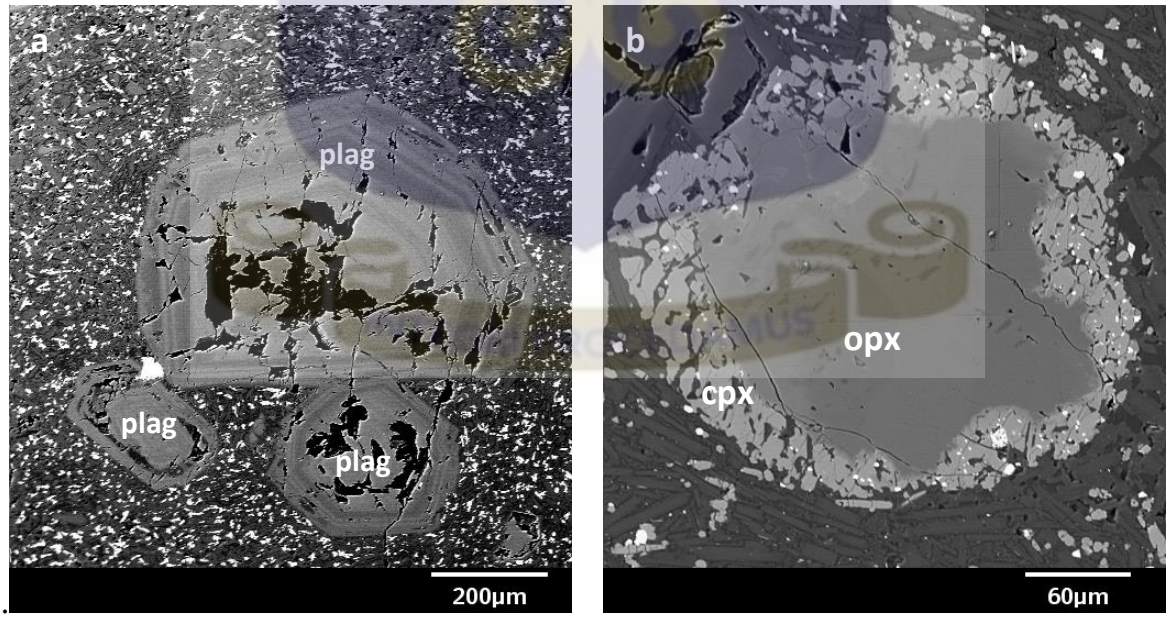

Fig. 4.3: Back-scattered electron image of Coromandel Andesite (a) Internally embayed plagioclase crystals. (b) Orthopyroxene (opx) crystal with clinopyroxene rim. Rim contains Ti-magnetite inclusions (whitish inclusions).

The hornblende crystals are anhedral to subhedral in form with crystal measuring up to 3 mm. They have coronas measuring up to 100 microns. The crystals also occur in glomeroporphyritic aggregates. The glomeroporphyritic crystals are petrographically similar to single crystals in the same rock. The glomeroporphyritic aggregates are surrounded by a zone in which the matrix contains a high concentration of single crystals, which appear similar to the crystals that comprise the aggregate.

4.2.1 Plagioclase-pyroxene andesite

It has a porphyritic- aphanitic texture (Fig. 4.4) with a phenocryst content of about 55%. It contains plagioclase (25%), pyroxene (15%), olivine (5%), hornblende (5%) and opaque minerals (5%). The plagioclase crystals have a euhedral to subhedral lath-shape. Clinopyroxene lamellae were seen within some of the plagioclase crystals. The pyroxenes are euhedral to subhedral and are altered to chlorite in some places. Orthopyroxene crystals mantled by clinopyroxene are present in this rock type.

The olivine crystals are euhedral to subhedral with both large and relatively small crystals. The amphibole crystals were also euhedral to subhedral in shape. They had thick opaque rims (0.4mm) measuring up to 0.4mm. The opaque rims had plagioclase inclusions. Ti-

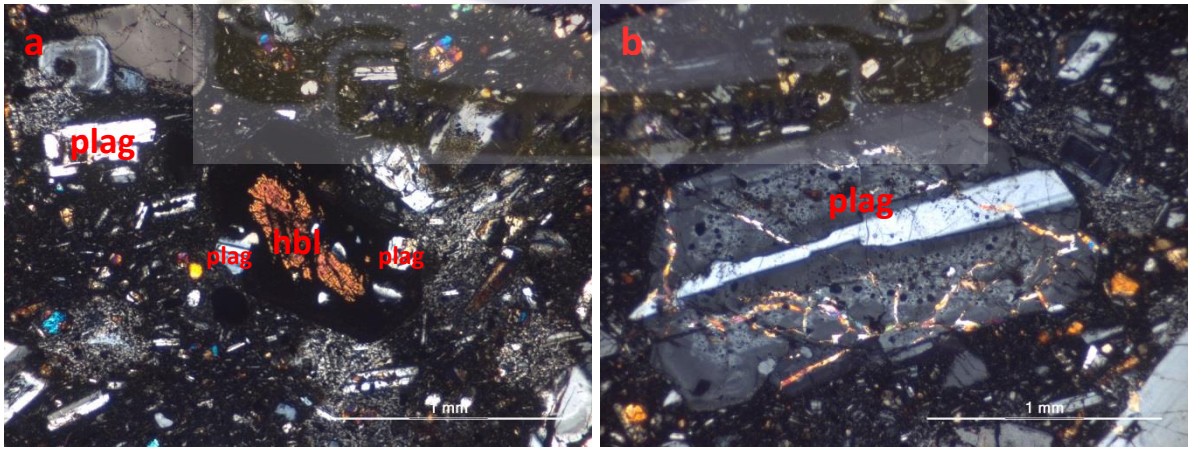

Fig. 4.4 Photomicrographs of plagioclase-pyroxene andesite (a) Amphibole with opaque rim having plagioclase inclusions (XPL). (b) Plagioclase with sieve textured core and clinopyroxene lamellae (XPL).

magnetite crystals were present in euhedral to subhedral form. They were dark under cross polarised light but white under plane polarised light. The rock was observed at stations 14-CP-04, 14-CP-05, 14-CP-07, 14-CP-17, 14-CP-20, 14-CP-28 and 14-CP-30.

4.2.2 Plagioclase- hornblende andesite

It has a porphyritic- aphanitic texture with a phenocryst content of about 50%. It contains Plagioclase (30%), Hornblende (15%), Pyroxene (5%). The plagioclase crystals are euhedral to subhedral. It also shows concentric zoning and polysynthetic twinning. The hornblende crystals are euhedral. They are greenish in color with portions of it altered to opaque coloration. The amphibole crystals also show reaction rims around them (Fig 4.5). Other rock fragments (xenocrysts) were seen in this rock (fig 4.5). This rock type was observed at stations 14-CP-06B, 14-CP-06D, 14-CP-10A, 14-CP-10B and 14-CP-16.

4.2.3 Hornblende- plagioclase andesite

This group of rocks have a porphyritic texture with 45% phenocryst content. It contains hornblende (20%), plagioclase (15%), pyroxene (5%) and olivine (5%). The hornblende crystals are euhedral to subhedral in form with opaque rims and internal fractures with

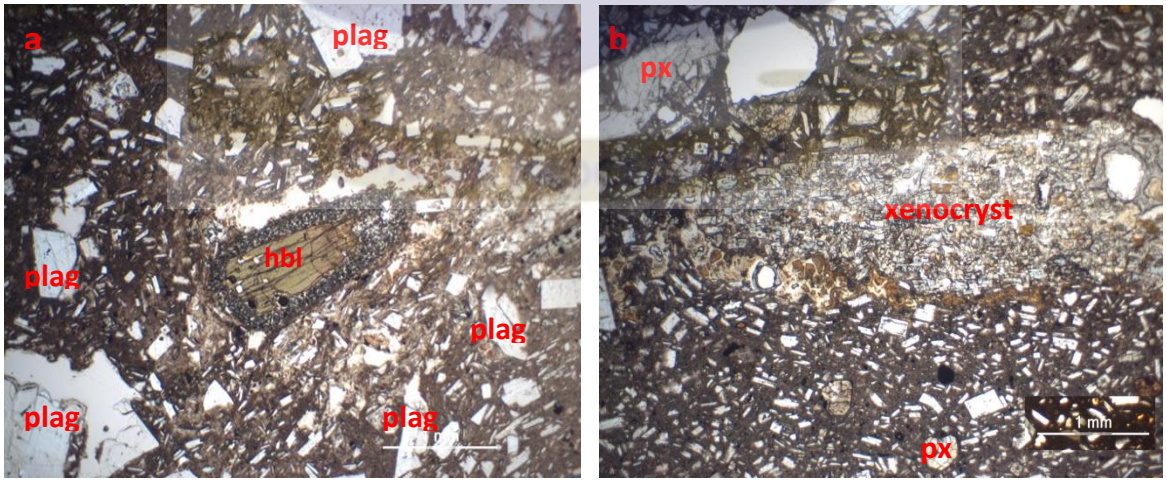

Fig. 4.5: photomicrographs of plagioclase-hornblende andesite (a) Amphibole crystal with reaction rim (PPL). (b) Xenocryst within the rock, suspected to be coming from the basement rock (PPL).

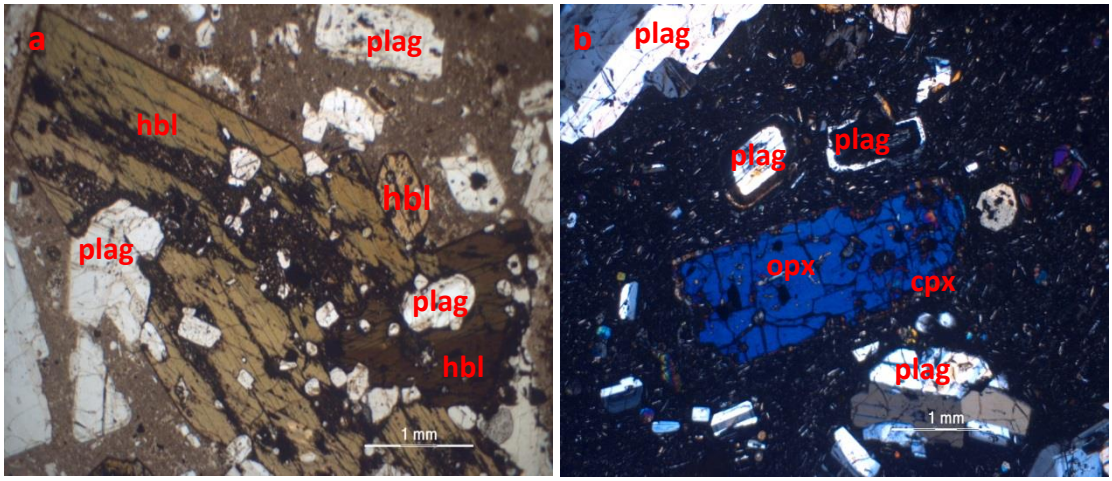

Fig. 4.6: photomicrographs of hornblende plagioclase andesite (a) Hornblende (hbl) with plagioclase inclusions (PPL). (b) Orthopyroxene with clinopyroxene rim (XPL).

alteration along them (Fig. 4.6). The amphiboles have plagioclase incusions and the crystals also occur in cumulophyritic aggregates. The cumulophyritic crystals are petrographically similar to single crystals in the same rock. The cumulophyritic aggregates are surrounded by a zone in which the matrix contains a high concentration of single crystals, which appear similar to the crystals that comprise the aggregate. The plagioclase crystals are euhedral to subhedral in form and shows polysynthetic twinning in two directions. Plagioclase with sieve textured core and unaltered rims are present. The sieve texture is also found in the mid portions of some crystals having unaltered core and rim. The pyroxene are euhedral to subhedral in form. They are ortho-pyroxenes with irregular cracks and have pyroxene inclusions. Most of the ortho-pyroxenes are mantled by clinopyroxene (Fig 4.6). Some also have opaque rims. The olivines are euhedral to subhedral in form. This rock type was observed at stations 14-CP-03A and 14-CP-26.

4.2.4 Hornblende- pyroxene andesite

It has a porphyritic- aphanitic texture (Fig. 4.7) with a phenocryst content of about 40-50%. It contains Hornblende (15%), pyroxene (15%), plagioclase (10%), olivine (5%) and opaque minerals (5%). The hornblende crystals are euhedral in form and large in size measuring up to 4 mm in length. They have cracks with slight alterations along them and thick reaction rims are found around some of them. Opaque rims and internal opaque spots are also present in them. The pyroxene crystals are euhedral to subhedral in form. The plagioclase crystals are euhedral in form and shows albite twinning and patchy zoning. They also have cracks along them. The opaque minerals are euhedral to subhedral in form. This rock type was observed at stations 14-CP-18, 14-CP-22 and14-CP-23.

4.2.5 Hornblende- pyroxene- plagioclase andesite

This rock type has a porphyritic texture with a phenocryst content of about 40-45%. Its composition includes mainly hornblende (15%), pyroxene (10%), plagioclase (10%) and olivine (5%). The hornblende crystals are euhedral to subhedral in form and have irregular cracks along them. The pyroxenes are euhedral in form with irregular fractures and alteration rims (fig. 4.8). The plagioclase crystals are euhedral to subhedral in form. They show zoning and twinning together with internal embayed spots. Boxy-cellular (Fig. 4.8) and sieve textured cores are also present. The olivine crystals are euhedral to subhedral in form. The sample was taken from station 14-CP-19.

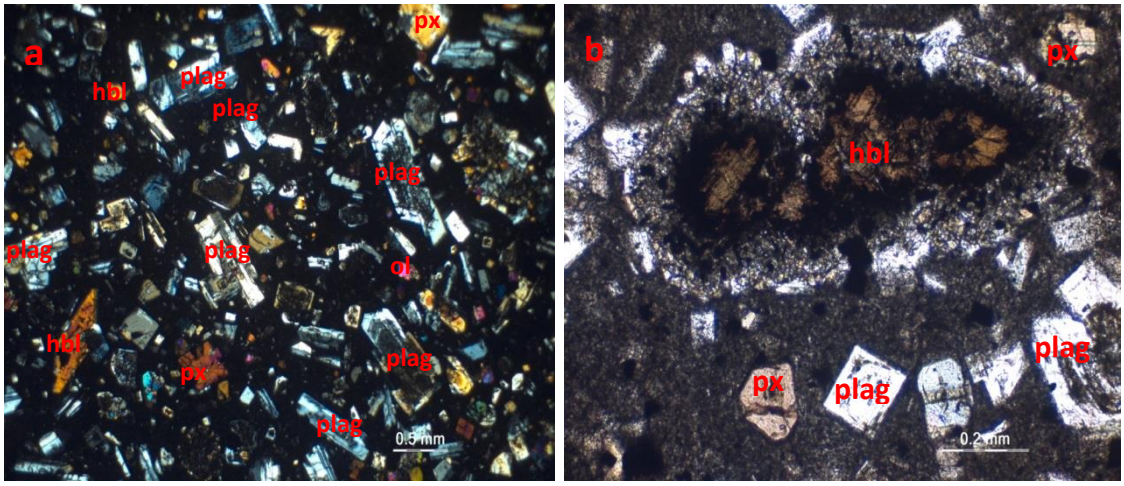

Fig. 4.7: photomicrographs of hornblende pyroxene andesite (a) slide showing minerals including plagioclase (plag) with deformed(sieve textured) core, hornblende(hbl), pyroxene(px) and olivine(ol)-XPL (b) Hornblende crystal with thick corona-PPL.

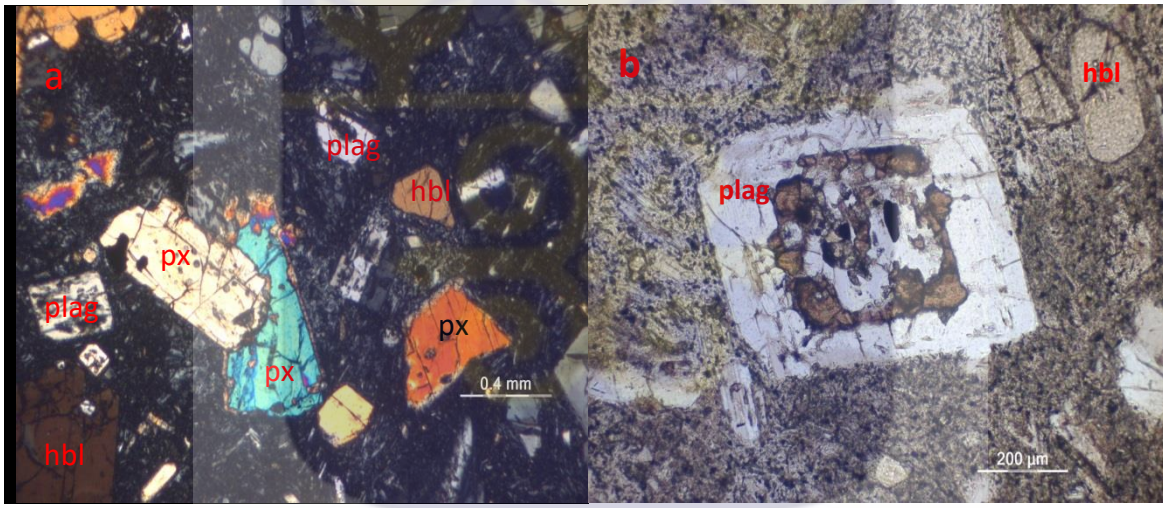

Fig. 4.8: photomicrographs of hornblende-pyroxene-plagioclase andesite (a) pyroxene with alteration rim(XPL). (b) plagioclase crystal with boxy cellular core (PPL).

The Kiwitahi andesite samples studied are from the Miranda and Tahuna centers. The older Miranda andesite has a more porphyritic texture as compared to the much younger Tahuna andesite. The Kiwitahi Miranda andesites studied are Hornblende-pyroxene- plagioclase andesites while the Tahuna andesites are plagioclase-pyroxene andesites. Their phenocryst content is 35-40% vol. comprising of plagioclase, pyroxene and olivine together with some xenocryst. The Plagioclase occurs as euhedral to subhedral crystals up to 2.5 mm in size. The crystals are typically zoned and show boxy-cellular and sieve textures (Fig. 4.9). The

boxy-cellular and sieve textures appear to be replacing the zoning. The pyroxene is typically euhedral to subhedral in form. Hornblende crystals are typically subhedral angular and opaque-rimmed. The younger Tahuna andesite are petrographically comparable to the andesites of the older centers, but lack hornblende.

4.2.6 Hornblende-plagioclase-pyroxene andesite

This rock type has a porphyritic texture with a phenocryst content of about 40-45%. The main composition includes hornblende (20%), pyroxene (15%) and plagioclase (20%). The hornblende crystals are subhedral in form with opaque rims. They also have inclusions. Some of the amphiboles have been altered to iron Ti- magnetite.

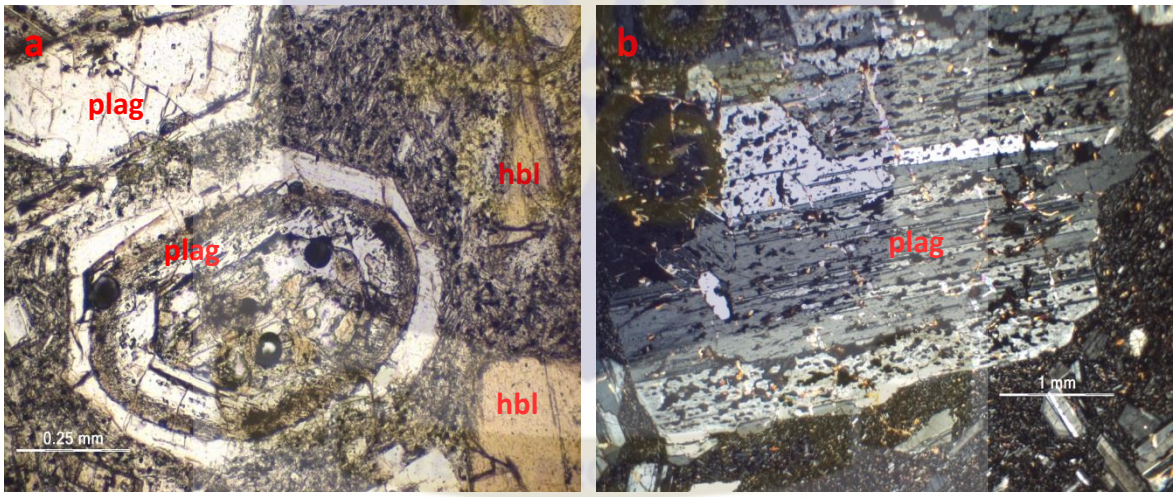

Fig. 4.9 Photomicrographs of Kiwitahi Andesites (a) plagioclase showing boxy-cellular texture (PPL). (b) Plagioclase showing twining and sieve textured core (XPL).

Fig. 4.10: photomicrographs of hornblende-plagioclase-pyroxene andesite. (a) plagioclase crystal showing concentric zoning and new growth rim. (b) Amphibole showing plagioclase inclusions and plagioclase showing twining.

The plagioclase crystals are euhedral to subhedral in form with a few crystals exhibiting concentric zoning (Fig. 4.10). Some of the crystals have pyroxene inclusions. Few of the crystals have embayed core and smooth rim. Some of the plagioclase crystals also show altered mid-section (indicating a previous rim) mantled by thin smooth rims (Fig. 4.10). The pyroxene crystals are euhedral to subhedral in form. The rock sample was taken from station 14-CP-38.

4.2.7 Plagioclase-pyroxene andesite

These rocks have a porphyritic texture with a phenocryst content of about 45%. The rocks contain plagioclase (20%), pyroxene (20%) and opaque minerals (5%). The plagioclase crystals are euhedral to subhedral in form. Albite twinning is present as well as sieve textured cores. Some have smaller pyroxene crystal inclusions in the core. There are plagioclase crystals with altered core and smooth rims whereas some crystals also show unaltered core, sieve textured mid-section and smooth unaltered thin rims mantling the

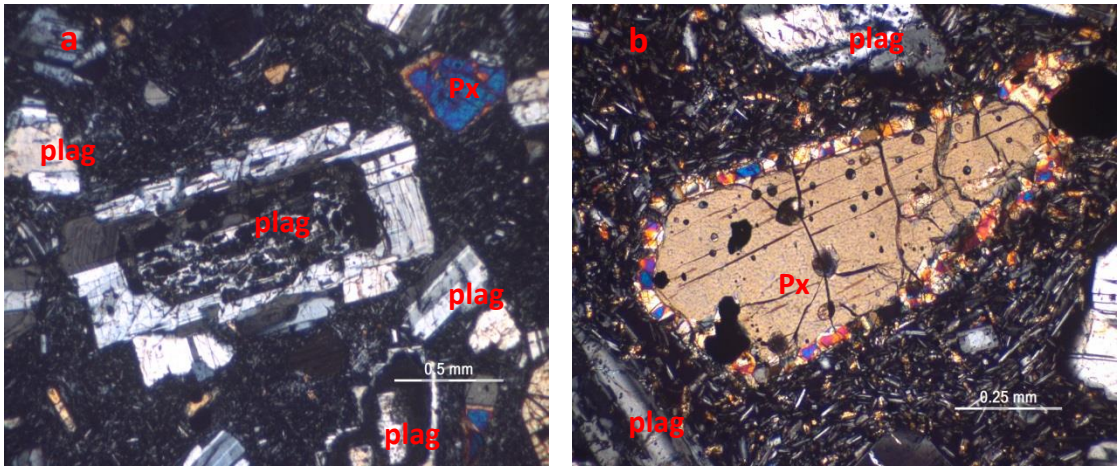

Fig. 4.11: photomicrographs of plagioclase-pyroxene andesite (a) A plagioclase with defomed core and smooth rims (XPL) (b) A pyroxene with a peculiar clinopyroxene rim(XPL).

alteration surface (Fig. 4.11). The pyroxenes are euhedral to subhedral in form. This sample was collected from areas 14-CP-34 and 14-CP-36B. The pyroxenes are mainly orthopyroxenes, they are euhedral to subhedral in form and range in size from 0.2-1.75 mm in length. They also have a peculiar rim around them. The rim is believed to be clinopyroxene. There is also the occurrence of a clinopyroxene crystal with an orthopyroxene rim.

4.2.8 The mercury basalts

These are of two types and they have been identified as olivine basalt and basaltic andesite (Skinner, 1976). Both of them were taken from the North eastern part of the study area thus they fall within the Coromandel Volcanic Zone.

4.2.8.1 Basaltic andesite

This rock has a porphyritic trachytic texture and consists of phenocryst make up of about 40-55% vol. The matrix consists of plagioclase microlites that have formed around the phenocrysts and appear to be flowing (Fig. 4.11). The phenocryst consists of plagioclase, pyroxene, olivine and opaque minerals. This sample was picked from station 14-CP-08.

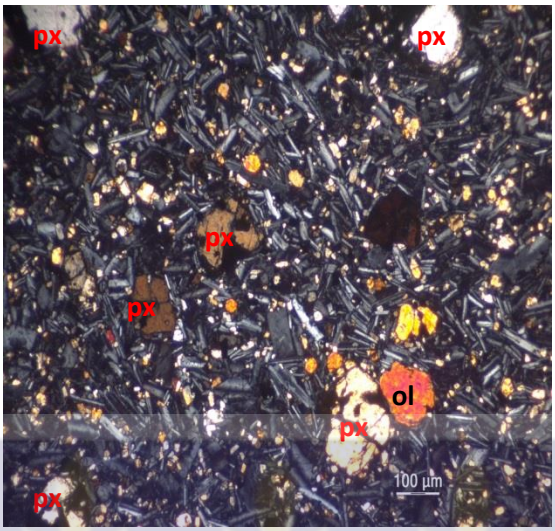

Fig 4.12: Photomicrograph of the basaltic andesite showing plagioclase, pyroxene, olivine and the trachytic texture (XPL).

The dominant mineral in the phenocryst is plagioclase (20-25% vol.). It is euhedral to subhedral in form with crystals measuring up to 1-2mm in size. Almost all the plagioclase crystals show patchy zoning and albite twinning. Most of the samples contain sieve texture in the core of the plagioclase crystals. Most of the feldspar crystals have clinopyroxene inclusions and lamellae.

The pyroxenes have subhedral rounded form and makes up about 10-15% vol. of the phenocryst. One peculiar characteristic of the pyroxenes in this rock type is the occurrence of an estimated 40-45 % of the orthopyroxenes mantled by clino-pyroxenes.

Olivine is present in this sample in varying crystal sizes measuring up to 1-5mm and makes up about 10-15% vol. of the rock. The crystals are subhedral to anhedral in form with irregular cracks which have alterations along them.

Hornblende is also present in very small quantity (5%) and euhedral to subhedral in form. They have opaque rims with plagioclase microlite inclusions.

4.2.8.2 Olivine basalt

This rock has an aphanitic microcrystalline trachytoid texture. It consists of about 45-50 % vol. of phenocryst. This sample was picked from station 14-CP-14. The phenocryst assemblage is plagioclase + pyroxene + olivine + hornblende + biotite.

The most abundant mineral plagioclase makes up 20-25 % vol. of the phenocryst. The olivine crystals here are uniformly spread out throughout the samples, they are subhedral rounded in form and makes up 10-12% vol. of the phenocryst. The Olivine crystals vary in size up to 100microns. The feldspar crystals are euhedral in form, lath-shaped and show alignment. The feldspar crystallites also show albite twinning. The pyroxenes are euhedral to subhedral in form and makes up about 3-5% vol. of the phenocryst. The hornblende crystallites are euhedral to subhedral in form and are < 1mm in size.

4.2.9 Dacite

This rock sample was taken from the central portion of the study area at station 14-CP-25. It has a porphyritic trachytic texture (Fig. 4.14) and made up of a phenocryst assemblage of plagioclase + pyroxene + Biotite + hornblende. It also has large quartz crystals surmised to be xenocrysts. The dacite consist of small phenocrysts of plagioclase feldspar that shows twinning (Fig. 4.15) and have reaction rim, hornblende, biotite and sparse pyroxene floating in a trachytic groundmass. The groundmass is made of plagioclase microlites with a trachytic texture. The phenocryst contains is 20-30% plagioclase, which is the dominant mineral in the rock.

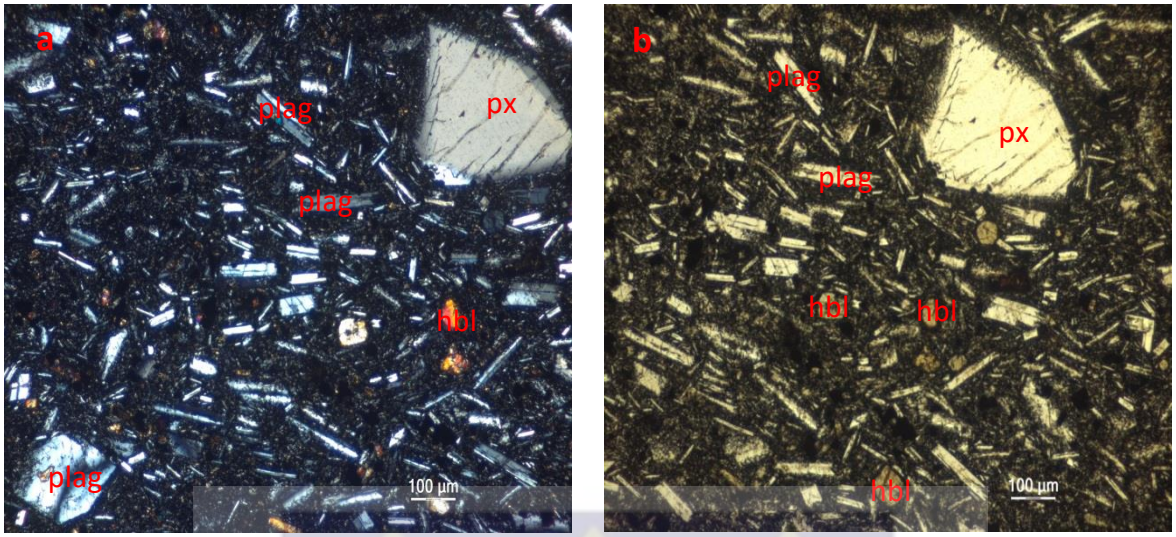

Fig 4.13 A and B: photomicrographs of basalt showing trachytoid matrix pyroxene (px), hornblende (hbl) and plagioclase (plag). a-XPL, b-PPL.

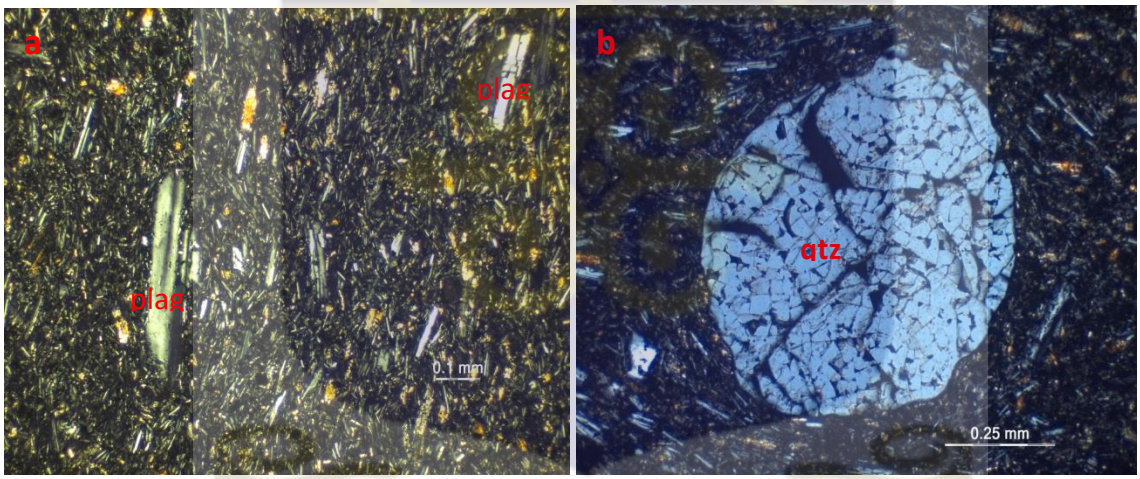

Fig 4.14a and 4.14b: photomicrographs of dacite. (a) shows the trachytoid texture and lath shaped plagioclase (plag) crystal (XPL). (b) Quartz (qtz) zenocryst found in the dacite.

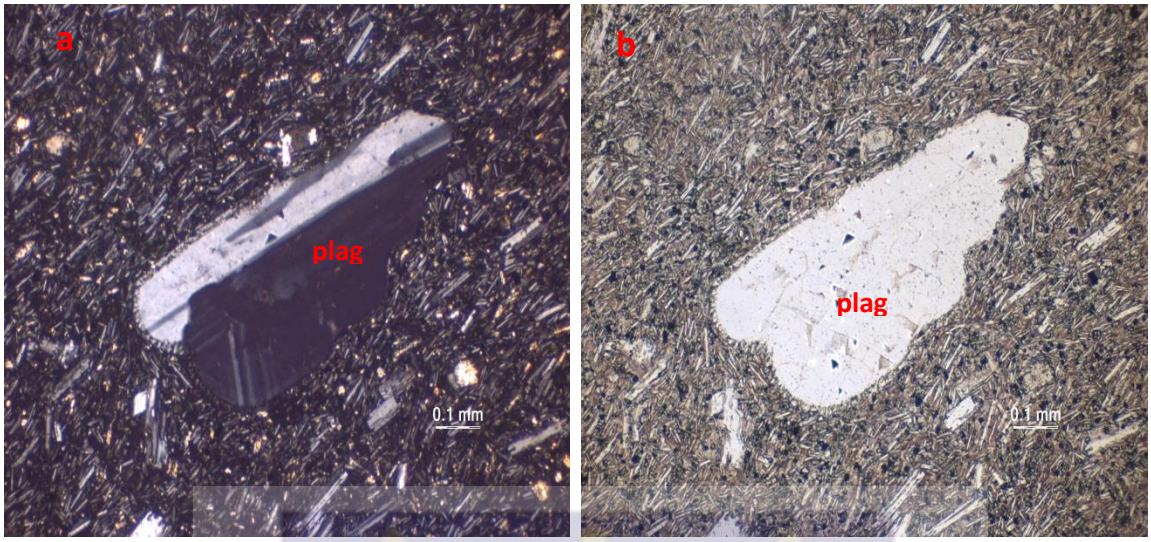

Fig 4.15: Photomicrograph of dacite showing plagioclase crystal with reaction rim. (a) plagioclase showing twinning-XPL (b) plagioclase crystal showing reaction rim-PPL.

4.3 MINERAL CHEMISTRY

The main minerals studied are the plagioclase and pyroxene crystals. Plagioclase and pyroxene were chosen for the mineral chemistry because they can preserve disequilibrium textures for long periods of time due to their slow ability to equilibrate. Thus, they are very good indicators of equilibrium and disequilibrium in a rock. Plagioclase is the dominant mineral phase in the rock sample studied thus the electron probe micro-analysis is focused mainly on the plagioclase mineral phase.

The pattern of chemical zoning exhibited by these minerals is the main focus. Zoning in the plagioclase crystals portrays differences in An-content. To study the configuration of chemical zoning shown by the plagioclase in the rock samples, an electron probe microanalysis has been performed across the mineral grains from the core to the rim of the zoned crystals. The geochemical traverses across three representative plagioclases and a zoned pyroxene are reported in table 1.

Fifteen (15) representative plagioclase crystals from the Coromandel andesite were analysed, overall the darker zones are more sodic than the lighter zones and the lighter zones are more calcic than the darker zones. Thus the Anorthite content fluctuated as the crystals were compositionally zoned. The lighter zones have relatively high calcium content (An_{62-78}) compared to the darker zones (An_{34-56}).

Generally, the plagioclase crystals of the representative samples show a more calcic core composition and a more sodic rim composition. Table 1 shows the data for two plagioclase crystals from the coromandel and their surrounding groundmass. The data presented is from core to rim (Fig. 4.17). The crystals have a high calcic composition (An_{81-82}) which falls within the average content (An_{72-82}), and is more calcic than surrounding mantle (An_{46-57}) and microlite in groundmass (An_{47-56}).

The surrounding mantle has anorthite content similar to that of the groundmass thus they are in equilibrium. The plagioclase crystals with boxy-cellular and sieve texture (Fig. 4.9) have a more calcic core composition (An_{72-80}) than the surrounding mantle (Table 4.1).

The pyroxenes show a range of textures from euhedral to anhedral resorbed. They also have rims (Fig 4.3b) that has abundant Ti-magnetite inclusions (45 crystals/mm^2, on average).

The BSE images show compositional zoning in the rims. Ten plagioclase crystals from Kiwitahi samples were analysed with the EPMA. The chemical analysis was done in groups namely the Coromandel Andesite, Kiwitahi Tahuna andesite and Kiwitahi Miranda andesite.

4.3.1 Coromandel andesite

In the zoned plagioclase crystals within the Coromandel andesite the lighter zones have a relatively high calcium content (An_{62-78}) compared to the darker zones (An_{34-56}).

The plagioclase crystals in the Coromandel show a variation in calcic content from zone to zone as shown in the graph (Fig. 4.16). The rim has anorthite content $An_{(68-67)}$ in the labradorite zone, similar to that of the groundmass thus they are in equilibrium (Fig. 4.17).

Table 4.1. EPMA data of representative samples from Coromandel Volcanic Zone, NE part of the study area. (from core to rim).

Sample	albite-pure	17-area1-plag1	17-area1-plag2	17-area1-plag3	17-area2-plag1	17-area2-plag2	17-area2-plag3	17-area2-plag4	17-area2-plag5	17-area2-plag6
SiO2	68.74	48.55	54.08	49.42	54.68	49.01	54.15	50.72	51.03	51.31
Al2O3	19.44	32.46	28.76	31.02	28.54	31.97	28.71	30.15	29.90	29.86
FeO		0.35	0.34	0.74	0.29	0.37	0.28	0.81	1.05	0.78
CaO		15.69	11.51	14.67	11.05	15.40	11.21	13.76	13.65	13.28
Na2O	11.82	2.40	4.67	2.99	4.94	2.58	4.79	3.40	3.62	3.71
K2O		0.10	0.37	0.19	0.32	0.09	0.24	0.19	0.26	0.26
Total	100.00	99.55	99.74	99.03	99.82	99.42	99.37	99.02	99.50	99.20
Si	3.00	2.23	2.45	2.28	2.47	2.25	2.46	2.34	2.34	2.36
Al	1.00	1.76	1.54	1.69	1.52	1.73	1.54	1.64	1.62	1.62
Fe	0.00	0.01	0.01	0.03	0.01	0.01	0.01	0.03	0.04	0.03
Ca	0.00	0.77	0.56	0.73	0.54	0.76	0.55	0.68	0.67	0.65
Na	1.00	0.21	0.41	0.27	0.43	0.23	0.42	0.30	0.32	0.33
K	0.00	0.01	0.02	0.01	0.02	0.01	0.01	0.01	0.02	0.02
∑ T cations	5.00	5.00	4.99	5.01	4.99	5.00	4.99	5.00	5.01	5.01
∑ cations	4.00	3.99	3.99	3.98	3.99	3.99	4.00	3.98	3.96	3.98
∑ alkali	1.00	0.99	0.99	1.01	0.99	0.99	0.98	0.99	1.01	1.00
Ab	100.00	21.54	41.38	26.62	43.85	23.16	42.95	30.52	31.93	33.06
An	0.00	77.85	56.44	72.27	54.25	76.30	55.62	68.34	66.57	65.43
Or	0.00	0.61	2.18	1.10	1.89	0.55	1.43	1.14	1.50	1.51

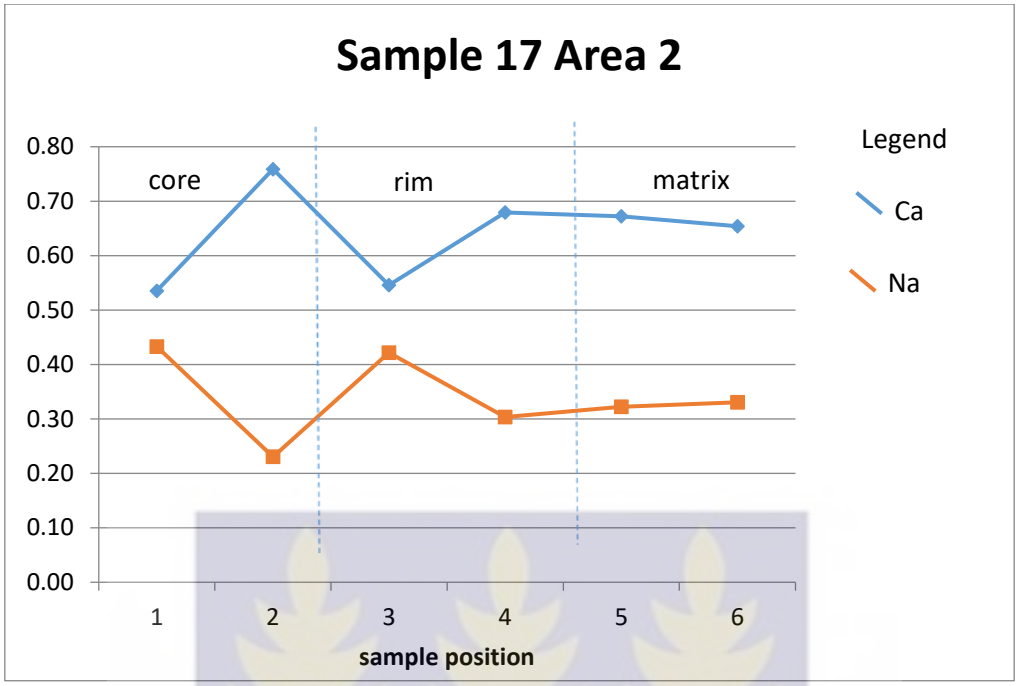

Fig 4.16: Variation of Ca and Na in the Coromandel andesite

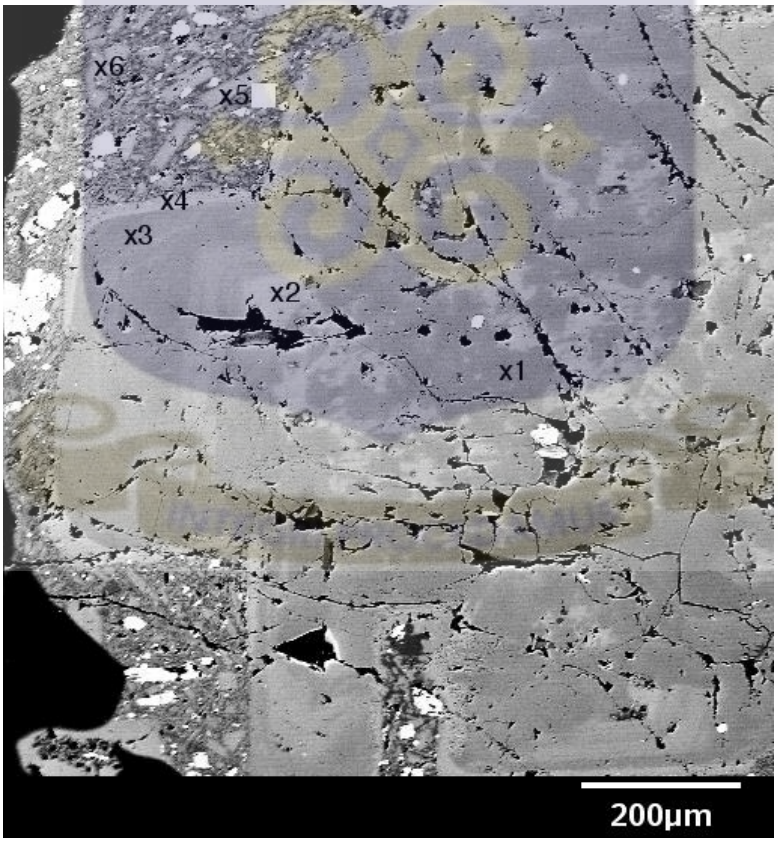

Fig 4.17: Back-scattered Electron image showing traverse point along a plagioclase in a Coromandel andesite (sample17, area 2)

4.3.2 Kiwitahi miranda andesite

The traverse path for the analyses of the representative plagioclase crystal discussed here is shown in Fig. 4.19. The zoned plagioclase crystals in the Kiwitahi Miranda andesite mainly shows a uniform calcic and sodic content from core to mid-section (Fig. 4.18), with an Anorthite content of An (48-50), placing the portion of the crystal in the Andesine zone. The rim on the other hand has a higher calcic content and lower sodic content. The Anorthite content of the rim is in the range of An (57-66). This places the rim in the Labradorite zone.

Table 4.2: EPMA data of representative samples from Kiwitahi Miranda, Southwestern part of the study area (From core to rim).

Sample	albite-pure	38-area2-plag1	38-area2-plag2	38-area2-plag3	38-area2-plag4	38-area2-plag5	38-area3-plag1	38-area3-plag2	38-area3-plag3	38-area3-plag4	38-area4-plag1	38-area4-plag2	38-area4-plag3	38-area4-plag4
SiO2	68.74	55.29	56.36	56.75	57.70	54.29	56.05	52.3	56.7	52.4	55.96	57.05	55.87	52.03
Al2O3	19.44	27.67	27.03	26.38	26.68	28.40	27.21	30.0	26.7	29.3	26.99	26.77	27.53	30.11
FeO		0.37	0.16	0.23	0.20	0.35	0.25	0.3	0.2	0.5	0.22	0.17	0.23	0.48
CaO		10.47	9.76	9.42	9.45	11.47	10.27	13.3	9.7	12.8	9.86	9.68	10.32	13.28
Na2O	11.82	5.06	5.31	5.50	5.85	4.69	5.35	3.7	5.6	3.9	5.53	5.59	5.36	3.67
K2O		0.26	0.24	0.25	0.28	0.23	0.27	0.1	0.3	0.2	0.28	0.29	0.27	0.12
Total	100.00	99.11	98.85	98.52	100.16	99.45	99.40	99.7	99.2	99.1	98.85	99.55	99.56	99.69
Si	3.00	2.51	2.56	2.58	2.58	2.47	2.54	2.4	2.6	2.4	2.54	2.57	2.53	2.37
Al	1.00	1.48	1.44	1.41	1.41	1.52	1.45	1.6	1.4	1.6	1.45	1.42	1.47	1.62
Fe	0.00	0.01	0.01	0.01	0.01	0.01	0.01	0.0	0.0	0.0	0.01	0.01	0.01	0.02
Ca	0.00	0.51	0.47	0.46	0.45	0.56	0.50	0.7	0.5	0.6	0.48	0.47	0.50	0.65
Na	1.00	0.45	0.47	0.48	0.51	0.41	0.47	0.3	0.5	0.3	0.49	0.49	0.47	0.32
K	0.00	0.02	0.01	0.01	0.02	0.01	0.02	0.0	0.0	0.0	0.02	0.02	0.02	0.01
∑ cations	5.00	4.98	4.96	4.96	4.98	4.99	4.98	5.0	5.0	5.0	4.98	4.97	4.98	4.99
∑ cations	4.00	3.99	4.00	4.00	3.99	3.99	3.99	4.0	4.0	4.0	3.99	3.99	3.99	3.99
∑ cations	1.00	0.97	0.95	0.96	0.98	0.99	0.98	1.0	1.0	1.0	0.98	0.97	0.98	0.98
Ab	100.00	45.92	48.89	50.60	51.98	41.97	47.76	32.8	49.9	35.0	49.54	50.22	47.70	33.09
An	0.00	52.51	49.68	47.89	46.38	56.68	50.68	66.3	48.3	63.9	48.78	48.08	50.75	66.18
Or	0.00	1.58	1.44	1.51	1.64	1.35	1.56	0.9	1.8	1.1	1.67	1.70	1.55	0.74

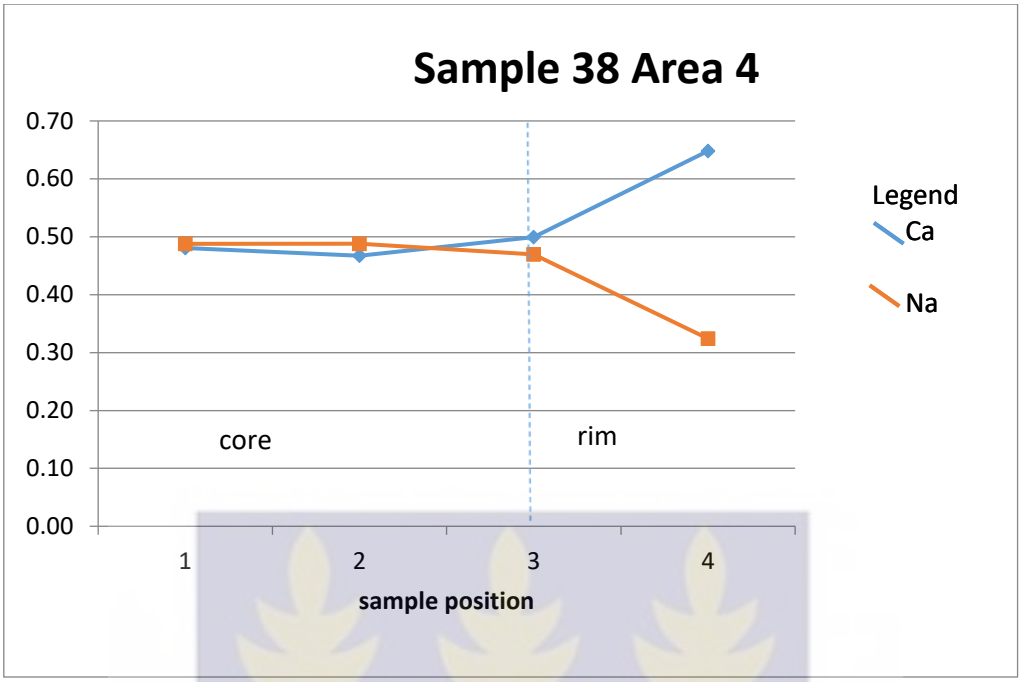

Fig 4.18: Variation of Ca and Na in the Kiwitahi Miranda andesite. This is a representation of the area 4 data in Table 2.

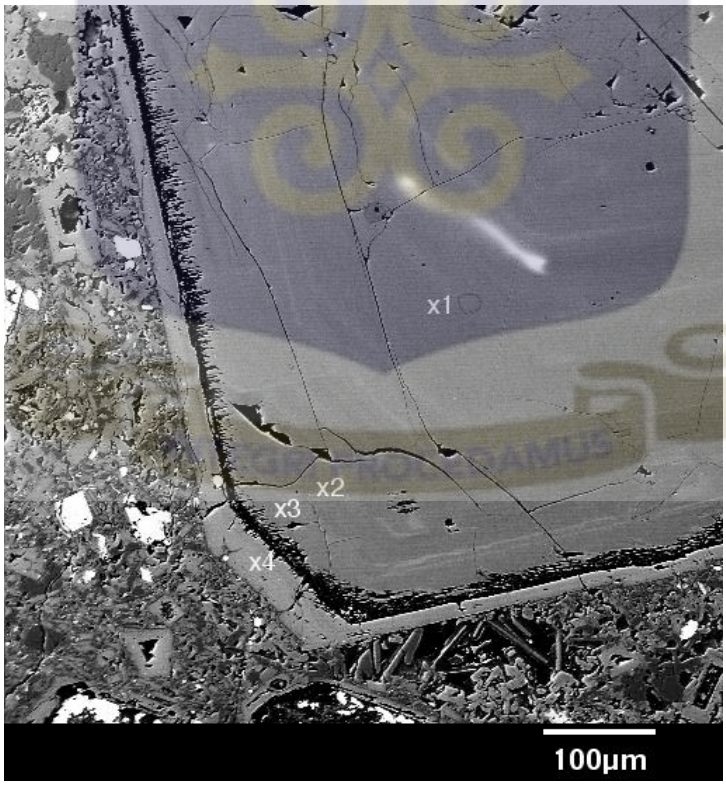

Fig. 4.19: Back-scattered Electron image showing traverse point along a plagioclase in a Kiwitahi Miranda andesite sample (sample 38, area 4).

4.3.3 Kiwitahi Tahuna andesite

The plagioclase crystals have high Ca content with An $_{(75\text{-}85)}$, the matrix has anorthite content of An$_{(\ 50\text{-}51)}$, which is different from the anorthite content of the crystals. A very unique characteristic of the Kiwitahi Tahuna is the very high calcic content of the core An $_{(75\text{-}80)}$, which drops slightly at the rim (Fig. 4.20). Almost all the crystals are in the bytownite zone. The rim has a lower Ca content with An$_{(75\text{-}43)}$. The matrix has a characteristic low calcic content of An$_{(50\text{-}51)}$. Fig. 4.21 shows the path of traverse of one of the chemical analysis.

Table 4.3: Plagioclase crystal chemistry data for the Kiwitahi- Tahuna Andesite. (From core to rim)

Sample	albite-pure	30-area1 plag1	30-area1 plag2	30-area1 plag3	30-area1 plag4	30-area1 plag5	30-area2-plag1	30-area2-plag2	30-area2-plag3	30-area2-plag4	30-area2-plag6	30-area2-plag7-matrix	30-area2-plag8matrix
SiO2	68.74	48.59	49.58	50.18	58.09	56.80	47.10	46.16	48.62	47.40	49.71	55.41	55.45
Al2O3	19.44	32.54	31.82	31.75	26.03	24.94	34.07	33.87	32.19	33.35	31.80	27.09	27.27
FeO		0.47	0.45	0.41	0.87	1.36	0.35	0.34	0.44	0.43	0.49	1.04	0.85
CaO		16.11	15.82	15.31	8.71	8.29	17.46	17.36	15.86	16.88	15.24	10.24	10.13
Na2O	11.82	2.23	2.43	2.70	6.12	6.22	1.56	1.66	2.49	1.94	2.74	5.24	5.13
K2O		0.09	0.12	0.13	0.43	0.44	0.05	0.05	0.09	0.05	0.10	0.38	0.32
Total	100.00	100.03	100.21	100.47	100.26	98.04	100.59	99.44	99.68	100.04	100.09	99.41	99.15
Si	3.00	2.23	2.26	2.28	2.60	2.61	2.15	2.14	2.24	2.18	2.27	2.52	2.52
Al	1.00	1.76	1.71	1.70	1.38	1.35	1.84	1.85	1.74	1.81	1.71	1.45	1.46
Fe	0.00	0.02	0.02	0.02	0.03	0.05	0.01	0.01	0.02	0.02	0.02	0.04	0.03
Ca	0.00	0.79	0.77	0.75	0.42	0.41	0.86	0.86	0.78	0.83	0.75	0.50	0.49
Na	1.00	0.20	0.22	0.24	0.53	0.55	0.14	0.15	0.22	0.17	0.24	0.46	0.45
K	0.00	0.01	0.01	0.01	0.02	0.03	0.00	0.00	0.01	0.00	0.01	0.02	0.02
∑ cations	5.00	5.00	4.99	4.99	4.99	5.00	5.00	5.01	5.01	5.01	5.00	5.00	4.98
∑ cations	4.00	3.98	3.98	3.98	3.98	3.96	3.99	3.99	3.98	3.98	3.98	3.97	3.98
∑ cations	1.00	0.99	1.00	0.99	0.98	0.99	1.00	1.01	1.01	1.01	0.99	0.98	0.97
Ab	100.00	19.91	21.62	24.03	54.58	56.11	13.87	14.72	21.99	17.14	24.40	47.01	46.92
An	0.00	79.58	77.69	75.24	42.89	41.30	85.81	84.99	77.50	82.59	75.02	50.76	51.18
Or	0.00	0.51	0.69	0.73	2.53	2.59	0.32	0.29	0.51	0.27	0.59	2.23	1.90

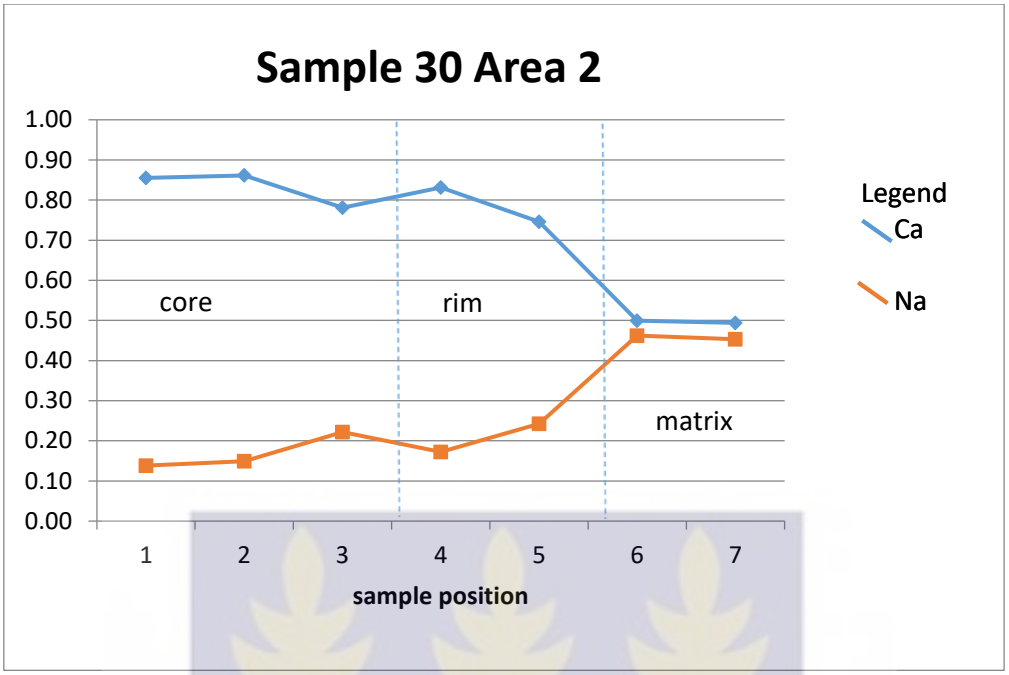

Fig. 4.20: Variation of Ca and Na in the Kiwitahi Tahuna andesite. This is a representation of the area 2 data in table 3.

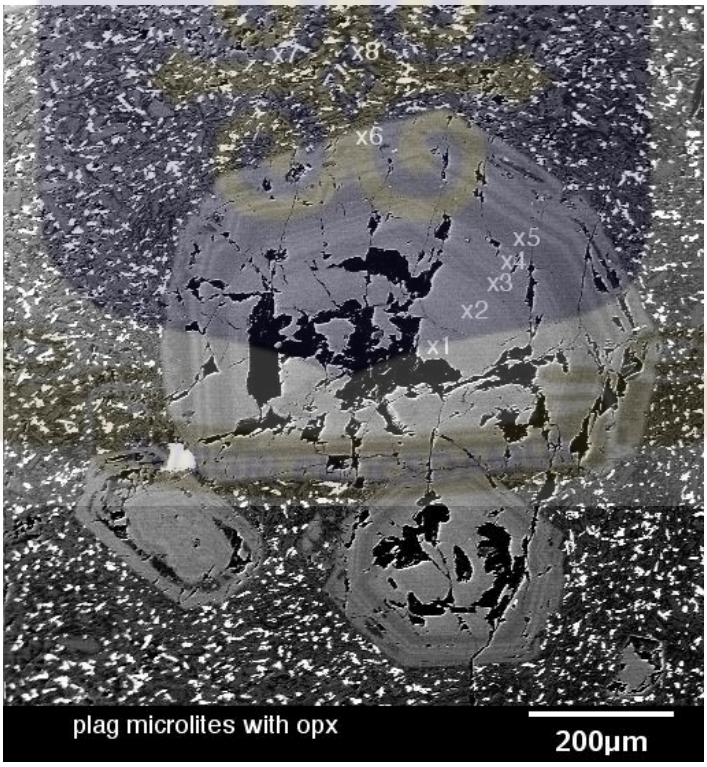

Fig. 4.21: Back-scattered Electron image showing traverse path along a plagioclase in a Kiwitahi Tahuna andesite sample (sample 30, area 2).

CHAPTER FIVE

DISCUSSION

Both the Coromandel group and Kiwitahi andesites are typically porphyritic with a phenocryst assemblage (20–60%) consisting of plagioclase + pyroxene + Fe –Ti-oxide in a granular groundmass rich in plagioclase laths and pyroxene microcrystals. Plagioclase is the dominant mineral in the samples and occurs as euhedral or subhedral crystals up to 2-3 mm in size, some of which show complex internal structure (Booden, 2011).

The Coromandel consists mainly of andesites, dacites and basalts. The Andesites are mainly plagioclase- pyroxene andesite, plagioclase- hornblende andesite, hornblende- plagioclase andesite, hornblende- pyroxene andesite and hornblende-pyroxene- plagioclase andesite.

The CVZ volcanic system involves a progression from an initial stage of andesitic volcanism to an evolved stage with rhyolitic volcanism. This progression occurred repeatedly in locations progressively farther to the south and east (Adams et al., 1994; Briggs et al., 2005).

Thus the volcanism can be proposed to have occurred over a magmatic system where a lower crustal hot zone had developed, in which andesitic magmas formed by the mixing of evolved, silicic melts or magmas, partly comprising crustal material, and mafic magmas or crystal assemblages with an overall mafic composition.

The Kiwitahi Miranda sample is an andesite, specifically a hornblende-pyroxene-plagioclase andesite, while the Kiwitahi Tahuna sample is also an andesite but a plagioclase-pyroxene andesite.

The Coromandel hornblende-pyroxene-plagioclase andesite has an $An_{(55-77)}$ which places it within the bytownite and labradorite zones whiles the Kiwitahi Miranda hornblende-

pyroxene-plagioclase has $An_{(46-66)}$, thus placing the rock in the Labradorite and andesine zones. The hornblende-pyroxene-plagioclase in the Kiwitahi and Coromandel both overlap in the Labradorite zone. They are either formed from different magma sources or the same source that has undergone changes probably due to magma mixing or assimilation.

One major observation is that the younger Tahuna andesites are petrographically comparable to the andesites of the older centers, but lack hornblende as stated by Booden (2011).

Also, the Kiwitahi eruptions are widely separated in time, thus it is very likely that the magmas forming the different centers are not directly genetically related to each other.

The Kiwitahi Tahuna plagioclase crystals have a very high calcic content in the core $An_{(75-80)}$, which drops slightly at the rim. Almost all the crystals are in the bytownite zone. The rim has a lower Ca content with An $_{(43-75)}$, which is a characteristic of normal zoning. The matrix has a characteristic low calcic content of $An_{(50-51)}$. The characteristic low An content of the plagioclase crystallites in the matrix which is so different from that of the plagioclase crystals indicates that the conditions under which the crystals were formed was different from that under which the matrix was formed therefore, the system was in a state of disequilibrium at a certain point in time.

Disequilibrium features including internal resorption surfaces and growth rims that are either rich or lacking in inclusions occur in them. Subordinate olivine crystals also occur in the andesites whiles quartz and biotite crystals are seen in the dacites.

Disequilibrium condition are also confirmed in the rocks in the study area based on the occurrence of oscillation zoning in the plagioclase, boxy-cellular and sieve textures in the plagioclase crystals (Perugini et al., 2003).

Oscillatory zoning in the plagioclase crystals occurs as a result of growth of the crystal within convection currents in a magma chamber such that circulation causes quasi-regular changes in temperature and pressure. The zoning is observed in the plagioclase phenocrysts within the dacites and all the andesites. Boxy-cellular texture is also indicative of disequilibrium because it is formed when a normally zoned outermost rim develops around the affected crystal (Perugini et al, 2003).

For the sieve texture they are basically observed to be replacing the old oscillatory growth zones which implies dissolution of the feldspar thus infer disequilibrium in the rock. Some large crystals have internal fracture planes along which glassy patches occur. These features indicate that plagioclase crystals in the andesite samples experienced disequilibrium conditions resulting in small amounts of resorption by the surrounding melt. This is because resorption surfaces are generally characteristic of changes in temperature, pressure, melt composition and water content in the magma at large scale (Davidson and Tepely, 1997) whiles minor resorption surfaces are attributed to local effects of minor changes in the same parameters as a result of magma dynamic for instance magma recharge (Perugini, 2003).

Glomeroporphyritic aggregates are common in the samples studied and are observed amongst amphibole (CP-03A) and plagioclase crystals (CP- 17, CP-28, etc). Most of the glomeroporphyritic aggregates are surrounded by a zone in which the matrix contains a high concentration of single crystals of the same mineral, with characteristics similar to the crystals that comprise the aggregate.

These features indicate that the crystals in many andesite samples are fragments derived from larger crystals and/or from disaggregated glomeroporphyritic crystal aggregates, suggesting that they are part of a remobilized crystal fraction. Where this is the case, the

crystals and the melt that entrains them are not necessarily genetically related and the bulk rock composition may not represent a melt composition.

The pyroxene crystals with their rims and its associated Ti-magnetite inclusions that are restricted to the rims suggest that conditions of crystallization, such as temperature , differed from those that existed during precipitation of their cores (Simonetti et al., 1996).

The hornblende crystals are subhedral angular and opaque-rimmed, suggesting resorption by the melt, which is also indicative of disequilibrium. One major observation is that the younger Tahuna andesite are petrographically comparable to the andesites of the older centers, but lack hornblende as stated by Booden, (2011).

CHAPTER SIX

CONCLUSION

The porphyritic basaltic andesites, andesites and dacites of the Coromandel Group have bulk compositions that do not correspond to frequently occurring melt inclusion compositions, and have textural and crystal chemical properties that suggest that they comprise mixtures of melts and entrained crystal assemblages.

The younger Tahuna andesites are petrographically comparable to the Miranda, but lack hornblende.

Also, the Kiwitahi eruptions are widely separated in time, thus it is very likely that the magmas forming the different centers are not directly genetically related to each other.

The textures indicative of disequilibrium include boxy cellular textures, oscillatory zoning, resorbed surfaces and a combination of these were seen in individual plagioclase feldspar crystals as well as coronas around pyroxene crystals.

Magma mixing is considered as one of the main processes that can stimulate the disequilibrium phenomena as those seen in this study (Simonette et al.,1996), due to the sieve and boxy textures of the plagioclase crystals which is evidence, that undercooling of a more mafic magma occurred in contact with a cooler more evolved magma.

In addition to that, the occurrence of Ti-magnetite as inclusions in the sieve textured core of the plagioclase crystals, in the rims of the pyroxene and the boxy-cellular textures of the plagioclase indicate that variables such as temperature and composition of magma, changed significantly, thus this can be associated to the magma mixing.

The sieve texture in the plagioclase also favours a magmatic interaction process to explain the observed disequilibrium textures. Thus the samples study can be said to have undergone disequilibrium through magmatic interaction which can possibly be magma mixing.

REFERENCES

Adams, C.J., Maas, R., 2004. Age/isotopic characterisation of the Waipapa Group in Northland and Auckland, New Zealand, and implications for the status of the Waipapa Terrane. New Zealand Journal of Geology and Geophysics 47, 173–187.

Adams, C.J., Graham, I.J., Seward, D., Skinner, D.N.B., 1994a. Geochronological and geochemical evolution of late Cenozoic volcanism in the Coromandel Peninsula, New Zealand. New Zealand Journal of Geology and Geophysics 37, 359–378.

Adams, C.J., Skinner, D.N.B., Moore, P.R., 1994b. K–Ar ages of some late Cenozoic volcanic rocks on Great Barrier Island. New Zealand Journal of Geology and Geophysics 37, 379.

Allan Hewitt, 'Soils - The most extensive soils', Te Ara - the Encyclopedia of New Zealand, http://www.TeAra.govt.nz/en/soils/page-4 (accessed 4 April 2017)

Anderson, A. T., 1984. Probable relations between plagioclase zoning and magma dynamics, Fuego Volcano, Guatemala. American Mineralogist 69, 660–676.

Ballance, P.F., Ablaev, A.G., Pushchin, I.K., Pletnev, S.P., Birylina, M.G., Itaya, T., Follas, H.A., Gibson, G.W., 1999. Morphology and history of the Kermadec trench–arc– backarc basin–remnant arc system at 30 to 32°S: geophysical profile, microfossil and K-Ar data. Marine Geology 159, 35–42.

Ballance, P.F. and Campbell, J.D., 1993, The Murihiku arc-related basin of New Zealand (Triassic–Jurassic), in Ballance P. F. (ed), South Pacific sedimentary basins, Sedimentary Basins of the World 2: Elsevier, Amsterdam, pp. 21–33.

Black, P.M., 1967. Petrology of the Cuvier and Paritu plutons and their metamorphic aureoles. Thesis (PhD Thesis, [s.n.] Geology) — University of Auckland, 1967., Auckland, 354 l. pp.

Ballance,P.F.; Sporli, K.B. 1979: Northland Allochthon. Journal of the Royal Society 9: 259-275.

Black, P.M., Briggs, R.M., Itaya, T., Dewies, E.R., Dunbar, H. M., Kawasaki, K., Kuschel, E., Smith, I.E.M., 1992. K-Ar age data and geochemistry of the Kiwitahi Volca nics, western Hauraki Rift, Nor th Island, New Zealand. N. Z. J. Geol. Geophys. 35, 403– 413.

Booden, M.A., Smith, I.M., Mauk, J.L., and Black, P.M., 2012, Geochemical and isotopic development of the Coromandel volcanic zone, northern New Zealand, since 18 Ma: Journal of Volcanology and Geothermal Research, v. 219, p. 22,015–22,032.

Booden, M.A., 2011. Geochemical Development of the Late Cenozoic Arc Volcanism in Northland and the Coromandel, and Implications for Geochemical Exploration in the Hauraki Goldfeild. PhD thesis (unpublished).

Booden, M.A., Smith, I.E.M., Mauk, J.L., Black, P.M., 2010. Evolvi ng volcanism at the tip of a propagating arc: the earliest high-Mg andesites in northern New Zealand. Journal of Volcanology and Geothermal Research 195, 83– 96.

Brathwaite, R.L. and Christie, A.B., 1996. Geology of the Waihi area, Sheet T13BD & part U13, Scale 1:50 000. Geological Map, 21. Institute of Geological and Nuclear Sciences, Ltd., Wellington, N.Z.

Briggs, R.M., Houghton, B.F., McWilliams, M., Wilson, C.J.N., 2005. 40Ar/39Ar ages of silicic volcanic rocks in the Tauranga–Kaimai area, New Zealand: dating the transition between volcanism in the Coromandel Arc and the Taupo Volcanic Zone. New Zealand Journal of Geology and Geophysics 48, 459–469.

Carl Walrond, 'Natural environment - Geography and geology', Te Ara - the Encyclopedia of New Zealand, http://www.TeAra.govt.nz/en/natural-environment/page-1 (accessed 3 April 2017)

Carter, L., Shane, P., Alloway, B., Hall, I.R., Harris, S.E., Westgate, J.A., 2003. Demise of one volcanic zone and birth of another — A 12 m.y. marine record of rhyolitic eruptions from New Zealand. Geology 31, 493–496.

Crawford, A.J., Meffre, S., Symonds, P.A., 2003. 120 to 0 Ma tectonic evolution of the southwest Pacific and analogous geological evolution of the 600 to 220 Ma Tasman Fold Belt System. Geol. Soc. Am. Spec. Pap. 372, 383–403.

Davey, F.J., 1982. The structure of the South Fiji basin. Tectonophysics 87, 185–241.

Davidson, J.P., Tepley III, F.J., 1997. Recharge in volcanic systems; evidence from isotope profiles of phenocrysts. Science 275, 826–829.

DeMets, C., Gordon, R.G., Argus, D.F., Stein, S., 1994. Effect of revisions to the geomagnetic reversal time scale on estimates of current plate motions. Geophys. Res. Lett. 21, 2191–2194.

DiCaprio, L., Gurnis, M., Müller, R.D., and Tan, E., 2011, Mantle dynamics of continentwide Cenozoic subsidence and tilting of Australia: Lithosphere, v. 3, no. 5, p. 311–316, doi:10.1130/L140.1.

Dobosi, G., Fodor, R.V., 1992. Magma fractionation, replenishment, and mixing as inferred from green-core clinopyroxenes in Pliocene basanite, southern Slovakia. Lithos 28, 133–150.

Forbes, C., 1855. On the geology of New Zealand with notes on its carboniferous deposits QJGS 11: 521-30

Gaina, C., Müller, D.R., Royer, J., Stock, J., Hardebeck, J. and Symonds, P. (1998). The tectonic history of the Tasman Sea: A puzzle with 13 pieces. Journal of Geophysical Research 103: doi: 10.1029/98JB00386. issn: 0148-0227.

Hayward, B.W., Black, P.M., Smith, I.E.M., Ballance, P.F., Itaya, T., Doi, M., Takagi, M., Bergman, S., Adams, C.J., Herzer, R.H., Robertson, D.J., 2001. K–Ar ages of early Miocene arc-type volcanoes in northern New Zealand. New Zealand Journal of Geology and Geophysics 44, 285–311.

Herzer, R.H., 1995. Seismic stratigraphy of a buried volcanic arc, Northland, New Zealand and implications for Neogene subduction.Marine and Petroleum Geology 12, 511–531.

Herzer, R.H., Davy, B.W., Mortimer, N., Quilty, P.G., Chaproniere, G.C.H., Jones, C.M., Crawford, A.J., Hollis, C.J., 2009. Seismic stratigraphy and structure of the Northland

Plateau and the development of the Vening Meinesz transform margin, SW Pacific Ocean. Marine Geophysical Researches 30, 21–60.

Herzer, R.H., Mascle, J., Davy, B., Ruellan, E., Mortimer, N., Laporte, C., Duxfield, A., 2000. New constraints on the New Zealand– South Fiji Basin continent-back-arc margin. C. R. Acad. Sci. Paris, Sci. Terre Planet. 330, 701–708.

Hibbard, M. J., 1981. The magma mixing origin of mantled feldspars. Contributions to Mineralogy and Petrology 76, 158–170.

Hochstein, M.P., Ballance, P.F., 1993. Hauraki Rift: a young, active intra-continental rift in a back-arc setting. In: Ballance, P.F. (Ed.), South Pacific Sedimentary Basins. Elsevier, Amsterdam, pp. 293–305.

Huang, Y. M., Hawkesworth, C.J., van Calsteren, P., Smith, I., Black, P., 1997. Melting generation models for the Auckland volcanic field, New Zealand: constriants from U-Th isoltopes. Earth planet. Sci. Lett. 149, 67- 84.

Huang, Y.M., Hawkesworth, C., Smith, I., van Calsteren, P., Black, P., 2000. Geochemistry of late Cenozoic basaltic volcanism in Northland and Coromandel, New Zealand: implications for mantle enrichment processes. Chemical Geology 164, 219–238.

Luyendyk, B. P. 1995. Hypothesis for Cretaceous rifting of East Gondwana caused by subducted slab capture. Geology 23, 373–6.

Malengreau, B., Skinner, D., Bromley, C., Black, P., 2000. Geophysical characterisation of large silicic volcanic structures in the Coromandel Peninsula, New Zealand. New Zealand Journal of Geology and Geophysics 43, 171–186.

Mortimer, N., Herzer, R.H., Gans, P.B., Parkinson, D.L., Seward, D., 1998. Basement geology from Three Kings Ridge toWest Norfolk Ridge, southwest Pacific Ocean: evidence from petrology, geochemistry and isotopic dating of dredge samples. Mar. Geol. 148, 135–162.

Mortimer, N., Gans, P.B., Palin, J.M., Meffre, S., Herzer, R., Skinner, D.N.B., 2010. Location and migration of Miocene–Quaternary volcanic arcs in the SW Pacific region. Journal of Volcanology and Geothermal Research 190, 1–10.

Nicholson, K.N., Black, P.M., Hoskin, P.W.O., Smith, I.E.M., 2004. Silicic volcanism and back-arc extension related to migration of the Late Cainozoic Australian–Pacific plate boundary. Journal of Volcanology and Geothermal Research 131, 295–306.

Nixon, G. T., Pearce, T. H.,1987. Laser-interferometry study of oscillatory zoning in plagioclase: the record of magma mixing and phenocryst recycling in calc-alkaline magma chambers, Iztacchuatl volcano, Mexico. American Mineralogist 72, 1144–1162.

Pearce, J.A., Baker, P.E., Harvey, P.K., Luff, I.W., 1995. Geochemical evidence for subduction fluxes, mantle melting and fractional crystallisation beneath the South Sandwich island arc. Journal of Petrolology 36, 1073–1109.

Perugini, D., Busa, T, Poli, G., Nazzareni, S.,2003. The role of chaotic dynamics and flow fields in the development of disequilibrium textures in volcanic rocks. Journal of petrology 44,4. 733-756.

Richards, J.R., Cooper, J.A., Black, P.M., 1966. Potassium–argon age of plutonic intrusives on Cape Colville Peninsula and Cuvier Island, New Zealand. Nature 211, 725–726.

Rutherford, M.J., Hill, P.M., 1993. Magma ascent rates from amphibole breakdown: an experimental study applied to the 19 80– 19 86 Mount St . Helens eruptions. J. Geophys. Res. 98, 19,667– 19,685.

Simonetti, A., Shore, M., Bell, K., 1996. Diopside phenocrysts from nephelinite lavas, Napak volcano, Eastern Uganda: evidence for magma mixing. Canadian Mineralogist 34, 411–421.

Skinner, D.N.B., 1972. Subdivision and petrology of the Mesozoic rocks of Coromandel (Manaia Hill Group). New Zealand Journal of Geology and Geophysics 15, 203–227.

Skinner, D.N.B., 1976. Northern Coromandel. Scale 1:63 360. New Zealand geological survey geological map of New Zealand, sheet N40 and parts N35, N36 and N39. New Zealand Geological Survey.

Skinner, D.N.B., 1986. Neogene volcanism of the Hauraki Volcanic Region. Bull. R. Soc. N. Z. 21–47.

Skinner, D.N.B., 1993. Geology of the Coromandel Harbour area, Scale 1:50 000. Geological Map, 4. Institute of Geological and Nuclear Sciences, Ltd.

Skinner, D.N.B., 1995. Geology of the Mercury Bay area, scale 1:50 000. Geological Map, 17. Institute of Geological and Nuclear Sciences Ltd.

Smith, I.E.M., Ruddock, R.S., Day, R.A., 1989. Miocene arc-type volcanic/plutonic complexes of the Northland Peninsula, New Zealand. Bull. R. Soc. N. Z. 26, 205–213.

Sutherland, R., 1999. Basement geology and tectonic development of the greater New Zealand region: an interpretation from regional magnetic data. Tectonophysics 308, 341–362

Umino, S., Horio, A. 1998., Multistage magma mixing revealed in phenocryst zoning of the Yunokuchi pumice, Akagi volcano, Japan. Journal of Petrology 39, 101–124.

Whattam, S.A., Malpas, J., Ali, J.R., Smith, I.E.M., 2008. New SW Pacific tectonic model: cyclical intraoceanic magmatic arc construction and near-coeval emplacement along the Australia-Pacific margin in the Cenozoic. Geochem. Geophys. Geosyst. 9, Q03021.

Whattam, S.A., Malpas, J., Smith, I.E.M., Ali, J.R., 2006. Link between SSZ ophiolite formation, emplacement and arc inception, Northland, New Zealand: U–Pb SHRIMP constraints; Cenozoic SW Pacific tectonic implications. Earth Planet. Sci. Lett. 250, 606–632

Wilson, C.J.N., Houghton, B.F., McWilliams, M.O., Lanphere, M.A., Weaver, S.D., Briggs, R. M., 1995. Volcanic and structural evolution of Taupo Volcanic Zone, New Zealand: a review. J. Volcanol. Geotherm. Res. 68, 1–28.

Wright, I.C., Parson, L.M., Gamble, J.A., 1996. Evolution and interaction of migrating cross-arc volcanism and backarc rifting: an example from the southern Havre Trough (35°20'–37°S). J. Geophys. Res. 101, 22071–22086.

Wysoczanski, R.J., Todd, E., Wright, I.C., Leybourne, M.I., Hergt, J.M., Adam, C., Mackay, K., 2010. Backarc rifting, constructional volcanism and nascent disorganized spreading in the southern Havre trough backarc rifts (SW Pacific). J. Volcanol. Geotherm. Res. 190, 39–57.

APPENDICES

APPENDIX A. Supplementary Dataset for mineral chemistry. See Chapter 5 for analytical methods.

Table A1: Microprobe Data for feldspars analysed in Sample 3A (Hbl-plg andesite: Locality: Coromandel Volcanic zone (CVZ)).

Sample	albite-pure	3A-area1-zonedplag-1	3A-area1-zonedplag-2	3A-area1-zonedplag-3	3A-area1-zonedplag-4	3A-area2-zonedplag-1	3A-area2-zonedplag-2	3A-area2-zonedplag-3	3A-area2-zonedplag-4	3A-area2-zonedplag-5	3A-area2-zonedplag-6
SiO2	68.74	52.75	55.82	55.36	55.11	55.94	51.81	54.52	51.99	49.59	57.00
Al2O3	19.44	30.46	28.48	28.90	28.59	27.99	30.89	29.33	30.48	31.67	27.08
FeO		0.28	0.28	0.21	0.54	0.22	0.27	0.20	0.24	0.27	0.25
CaO		13.26	11.00	11.52	11.28	10.42	13.72	12.02	13.38	14.77	9.75
Na2O	11.82	4.15	5.33	5.11	5.14	5.75	3.61	4.60	3.98	3.00	6.01
K2O		0.08	0.09	0.10	0.18	0.11	0.07	0.09	0.07	0.05	0.14
Total	100.00	100.98	101.01	101.20	100.83	100.43	100.38	100.76	100.14	99.35	100.23
Si	3.00	2.37	2.49	2.47	2.47	2.51	2.35	2.44	2.36	2.28	2.56
Al	1.00	1.61	1.50	1.52	1.51	1.48	1.65	1.55	1.63	1.71	1.43
Fe	0.00	0.01	0.01	0.01	0.02	0.01	0.01	0.01	0.01	0.01	0.01
Ca	0.00	0.64	0.53	0.55	0.54	0.50	0.67	0.58	0.65	0.73	0.47
Na	1.00	0.36	0.46	0.44	0.45	0.50	0.32	0.40	0.35	0.27	0.52
K	0.00	0.00	0.01	0.01	0.01	0.01	0.00	0.00	0.00	0.00	0.01
∑ T cations	5.00	5.00	4.99	4.99	5.00	5.00	4.99	4.98	5.00	5.00	4.99
∑ cations	4.00	3.99	3.99	3.99	3.98	3.99	3.99	3.99	3.99	3.99	3.99
∑ alkali	1.00	1.01	0.99	1.00	1.00	1.01	0.99	0.98	1.00	1.00	1.00
Ab	100.00	36.01	46.45	44.28	44.72	49.67	32.13	40.72	34.86	26.82	52.31
An	0.00	63.55	53.01	55.12	54.26	49.72	67.44	58.78	64.76	72.88	46.89
Or	0.00	0.43	0.54	0.60	1.02	0.60	0.43	0.50	0.38	0.30	0.80

Table A2: Microprobe Data of Feldspars analysed in Sample 08 (Mercury Basalt; Locality:CVZ)

Sample	albite-pure	08-area1-plag1	08-area1-plag2	08-area2-plag1	08-area2-plag2	08-area2-plag3	08-area2-plag4
SiO2	68.74	54.75	53.66	51.19	60.21	51.25	53.95
Al2O3	19.44	27.40	27.96	29.83	24.19	29.97	28.17
FeO		0.87	0.95	1.06	0.73	0.90	1.04
CaO		10.73	11.65	13.63	6.47	13.68	11.48
Na2O	11.82	5.03	4.60	3.56	7.11	3.47	4.74
K2O		0.37	0.30	0.20	1.05	0.21	0.30
Total	100.00	99.62	99.11	99.48	99.76	99.48	99.69
Si	3.00	2.50	2.46	2.35	2.70	2.35	2.46
Al	1.00	1.47	1.51	1.61	1.28	1.62	1.51
Fe	0.00	0.03	0.04	0.04	0.03	0.03	0.04
Ca	0.00	0.52	0.57	0.67	0.31	0.67	0.56
Na	1.00	0.45	0.41	0.32	0.62	0.31	0.42
K	0.00	0.02	0.02	0.01	0.06	0.01	0.02
∑ T cations	5.00	5.00	5.00	5.01	5.00	5.00	5.01
∑ cations	4.00	3.97	3.97	3.97	3.98	3.97	3.97
∑ alkali	1.00	0.99	1.00	1.00	0.99	0.99	1.00
Ab	100.00	44.92	40.98	31.72	62.46	31.06	42.04
An	0.00	52.91	57.30	67.09	31.45	67.69	56.23
Or	0.00	2.17	1.73	1.19	6.09	1.24	1.73

Table A3: Microprobe Data of Feldspars analysed in Sample 17 (Andesite; Locality: CVZ)

Sample	albite-pure	17-area1-plag1	17-area1-plag2	17-area1-plag3	17-area2-plag1	17-area2-plag2	17-area2-plag3	17-area2-plag4	17-area2-plag5	17-area2-plag6
SiO2	68.74	48.55	54.08	49.42	54.68	49.01	54.15	50.72	51.03	51.31
Al2O3	19.44	32.46	28.76	31.02	28.54	31.97	28.71	30.15	29.90	29.86
FeO		0.35	0.34	0.74	0.29	0.37	0.28	0.81	1.05	0.78
CaO		15.69	11.51	14.67	11.05	15.40	11.21	13.76	13.65	13.28
Na2O	11.82	2.40	4.67	2.99	4.94	2.58	4.79	3.40	3.62	3.71
K2O		0.10	0.37	0.19	0.32	0.09	0.24	0.19	0.26	0.26
Total	100.00	99.55	99.74	99.03	99.82	99.42	99.37	99.02	99.50	99.20
Si	3.00	2.23	2.45	2.28	2.47	2.25	2.46	2.34	2.34	2.36
Al	1.00	1.76	1.54	1.69	1.52	1.73	1.54	1.64	1.62	1.62
Fe	0.00	0.01	0.01	0.03	0.01	0.01	0.01	0.03	0.04	0.03
Ca	0.00	0.77	0.56	0.73	0.54	0.76	0.55	0.68	0.67	0.65
Na	1.00	0.21	0.41	0.27	0.43	0.23	0.42	0.30	0.32	0.33
K	0.00	0.01	0.02	0.01	0.02	0.01	0.01	0.01	0.02	0.02
∑ T cations	5.00	5.00	4.99	5.01	4.99	5.00	4.99	5.00	5.01	5.01
∑ cations	4.00	3.99	3.99	3.98	3.99	3.99	4.00	3.98	3.96	3.98
∑ alkali	1.00	0.99	0.99	1.01	0.99	0.99	0.98	0.99	1.01	1.00
Ab	100.00	21.54	41.38	26.62	43.85	23.16	42.95	30.52	31.93	33.06
An	0.00	77.85	56.44	72.27	54.25	76.30	55.62	68.34	66.57	65.43
Or	0.00	0.61	2.18	1.10	1.89	0.55	1.43	1.14	1.50	1.51

Table A4: Microprobe Data of Feldspars analysed in Sample 19 (Hbl-pyr-plag andesite, Locality: CVZ)

Sample	albite-pure	19-area2-plag1	19-area2-plag2-small	19-area3-plag1	19-area3-plag2	19-area3-plag3	19-area3-plag4-matrix	19-area3-plag5-matrix	19-area3-plag6-matrix	19-area3-plag7-core
SiO2	68.74	50.54	60.72	50.23	54.22	50.54	51.42	55.33	53.77	52.25
Al2O3	19.44	31.07	23.90	31.19	28.53	31.35	30.10	28.30	28.90	29.55
FeO		0.58	0.81	0.55	0.46	0.52	0.64	0.42	0.72	0.51
CaO		14.37	6.64	14.87	11.43	14.96	13.90	11.03	12.14	12.93
Na2O	11.82	3.33	7.08	3.15	4.95	2.94	3.42	5.14	4.53	4.12
K2O		0.14	0.89	0.11	0.22	0.13	0.22	0.38	0.28	0.19
Total	100.00	100.03	100.04	100.10	99.81	100.44	99.70	100.60	100.34	99.55
Si	3.00	2.31	2.71	2.29	2.46	2.30	2.35	2.49	2.43	2.39
Al	1.00	1.67	1.26	1.68	1.52	1.68	1.62	1.50	1.54	1.59
Fe	0.00	0.02	0.03	0.02	0.02	0.02	0.02	0.02	0.03	0.02
Ca	0.00	0.70	0.32	0.73	0.56	0.73	0.68	0.53	0.59	0.63
Na	1.00	0.29	0.61	0.28	0.44	0.26	0.30	0.45	0.40	0.36
K	0.00	0.01	0.05	0.01	0.01	0.01	0.01	0.02	0.02	0.01
∑ cations	5.00	5.01	4.99	5.01	5.00	4.99	5.00	5.00	5.00	5.01
∑ cations	4.00	3.98	3.97	3.97	3.98	3.98	3.97	3.98	3.97	3.98
∑ cations	1.00	1.01	0.98	1.01	1.00	1.00	1.00	1.00	1.00	1.01
Ab	100.00	29.29	62.48	27.52	43.41	26.02	30.37	44.75	39.68	36.17
An	0.00	69.88	32.35	71.85	55.34	73.21	68.32	53.10	58.70	62.71
Or	0.00	0.83	5.17	0.64	1.26	0.76	1.31	2.15	1.62	1.12

Table A5: Microprobe Data Feldspars analysed in Sample 20 (Plag-pyr andesite; Locality: CVZ)

Sample	albite-pure	20-area1-plag1	20-area1-plag2	20-area1-plag3	20-area1-plag4	20-area1-plag5	20-area1-plag6	20-area1-plag7	20-area2-plag1	20-area2-plag2	20-area2-plag3
SiO2	68.74	55.00	51.59	55.14	56.23	51.81	69.69	68.96	51.58	53.95	53.80
Al2O3	19.44	28.41	30.63	28.91	28.05	30.25	20.43	20.17	31.10	28.62	29.10
FeO		0.41	0.43	0.40	0.32	0.84	0.02	0.00	0.42	0.39	0.44
CaO		11.54	14.42	11.96	10.88	14.33	1.08	0.91	14.44	12.04	12.61
Na2O	11.82	4.80	3.36	4.76	5.21	3.37	11.13	11.33	3.36	4.57	4.16
K2O		0.31	0.15	0.21	0.26	0.19	0.06	0.06	0.15	0.21	0.26
Total	100.00	100.47	100.57	101.38	100.95	100.79	102.40	101.43	101.06	99.79	100.36
Si	3.00	2.47	2.34	2.46	2.51	2.35	2.97	2.97	2.33	2.45	2.43
Al	1.00	1.51	1.64	1.52	1.48	1.62	1.03	1.02	1.65	1.53	1.55
Fe	0.00	0.02	0.02	0.01	0.01	0.03	0.00	0.00	0.02	0.01	0.02
Ca	0.00	0.56	0.70	0.57	0.52	0.70	0.05	0.04	0.70	0.59	0.61
Na	1.00	0.42	0.29	0.41	0.45	0.30	0.92	0.95	0.29	0.40	0.36
K	0.00	0.02	0.01	0.01	0.01	0.01	0.00	0.00	0.01	0.01	0.01
∑ cations	5.00	4.99	5.00	4.99	4.98	5.00	4.97	4.99	5.00	4.99	4.98
∑ cations	4.00	3.98	3.97	3.98	3.99	3.96	4.00	4.00	3.98	3.98	3.98
∑ cations	1.00	0.99	1.00	1.00	0.99	1.00	0.97	0.99	1.00	1.00	0.99
Ab	100.00	42.18	29.37	41.33	45.73	29.51	94.62	95.43	29.40	40.23	36.80
An	0.00	56.03	69.74	57.45	52.76	69.40	5.06	4.23	69.75	58.57	61.68
Or	0.00	1.78	0.88	1.23	1.51	1.09	0.32	0.35	0.85	1.19	1.52

Table A6: Microprobe Data Feldspars analysed in Sample 25 (Dacite; Locality: CVZ)

Sample	albite-pure	25-area1-plag1	25-area1-plag2
SiO2	68.74	54.16	57.26
Al2O3	19.44	27.76	26.00
FeO		1.07	1.02
CaO		11.51	10.16
Na2O	11.82	4.74	5.14
K2O		0.25	0.41
Total	100.00	99.49	99.99
Si	3.00	2.47	2.58
Al	1.00	1.49	1.38
Fe	0.00	0.04	0.04
Ca	0.00	0.56	0.49
Na	1.00	0.42	0.45
K	0.00	0.01	0.02
∑ cations	5.00	5.00	4.96
∑ cations	4.00	3.96	3.96
∑ cations	1.00	1.00	0.96
Ab	100.00	42.12	46.64
An	0.00	56.44	50.91
Or	0.00	1.44	2.46

Table A7: Microprobe Data Feldspars analysed in Sample 24 (Pyroxene andesite; Locality: Peninsula)

Sample	albite-pure	24-area1-plag1	24-area1-plag2	24-area1-plag3	24-area1-plag4	24-area1-plag-incl5	24-area1-plag-incl6	24-area2-plag1	24-area2-plag2	24-area2-plag3	24-area2-plag4	24-area3-plag1	24-area3-plag2	24-area3-plag3	24-area3-plagmatrix4	24-area3-plagmatrix5	24-area3-plagmatrix6	24-area3-plag-matrix8
SiO2	68.74	50.24	49.43	52.09	49.83	59.46	53.88	54.82	54.41	46.74	54.73	55.45	51.22	53.73	65.17	65.83	51.85	56.61
Al2O3	19.44	31.26	31.30	30.02	31.11	24.01	28.45	27.69	28.38	33.44	28.26	27.68	29.68	28.36	18.57	18.59	29.85	26.12
FeO		0.47	0.47	0.44	0.58	1.25	0.44	0.41	0.41	0.48	0.44	0.42	0.42	0.38	0.28	0.25	0.74	0.54
CaO		14.72	15.06	13.24	14.67	7.30	11.53	10.78	11.17	17.25	10.79	10.48	13.39	11.34	0.40	0.38	13.19	8.93
Na2O	11.82	3.00	2.86	3.80	2.95	6.63	4.77	5.14	5.10	1.67	5.22	5.33	3.85	4.84	4.31	4.02	3.93	5.66
K2O		0.15	0.13	0.18	0.16	0.53	0.30	0.37	0.27	0.04	0.28	0.25	0.14	0.33	10.13	10.33	0.24	0.55
Total	100.00	99.83	99.25	99.76	99.29	99.18	99.37	99.21	99.75	99.62	99.71	99.62	98.70	98.99	98.86	99.39	99.79	98.40
Si	3.00	2.30	2.28	2.37	2.29	2.69	2.45	2.50	2.47	2.16	2.48	2.51	2.36	2.46	2.99	3.00	2.37	2.58
Al	1.00	1.69	1.70	1.61	1.69	1.28	1.53	1.49	1.52	1.82	1.51	1.48	1.61	1.53	1.00	1.00	1.61	1.41
Fe	0.00	0.02	0.02	0.02	0.02	0.05	0.02	0.02	0.02	0.02	0.02	0.02	0.02	0.01	0.01	0.01	0.03	0.02
Ca	0.00	0.72	0.74	0.65	0.72	0.35	0.56	0.53	0.54	0.85	0.52	0.51	0.66	0.56	0.02	0.02	0.65	0.44
Na	1.00	0.27	0.26	0.34	0.26	0.58	0.42	0.45	0.45	0.15	0.46	0.47	0.34	0.43	0.38	0.36	0.35	0.50
K	0.00	0.01	0.01	0.01	0.01	0.03	0.02	0.02	0.02	0.00	0.02	0.01	0.01	0.02	0.59	0.60	0.01	0.03
∑ cations	5.00	5.00	5.00	4.99	5.00	4.98	5.00	5.00	5.01	5.01	5.00	4.99	5.01	5.00	5.00	4.98	5.01	4.98
∑ cations	4.00	3.98	3.98	3.98	3.98	3.97	3.98	3.98	3.98	3.98	3.99	3.99	3.98	3.98	3.99	4.00	3.97	3.99
∑ cations	1.00	1.00	1.01	0.99	1.00	0.96	1.00	1.00	1.01	1.01	1.00	0.99	1.01	1.00	1.00	0.97	1.01	0.97
Ab	100.00	26.68	25.35	33.80	26.42	60.20	42.06	45.34	44.52	14.84	45.90	47.20	33.97	42.75	38.47	36.47	34.56	51.68
An	0.00	72.45	73.86	65.15	72.65	36.62	56.19	52.53	53.92	84.90	52.46	51.33	65.20	55.34	1.98	1.89	64.06	45.03
Or	0.00	0.87	0.79	1.04	0.93	3.17	1.75	2.13	1.56	0.25	1.65	1.47	0.84	1.92	59.56	61.65	1.39	3.29

Table A8: Microprobe Data Feldspars analysed in Sample 28 (Plagioclase-pyroxene andesite; Locality: Tirohia quarry)

Sample	albite-pure	28-area2-plag1	28-area2-plag2	28-area2-plag3	28-area2-plag4	28-area2-plag5	28-area2-plag6	28-area2-plag7	28-area2-plag8	28-area3-plag1	28-area3-plag2	28-area3-plag3	28-area3-plag4	28-area3-plag5	28-area4-plag1	28-area4-plag2	28-area4-plag3	28-area4-plag4	28-area4-plag5
SiO2	68.74	48.25	48.37	50.49	49.48	53.10	59.77	54.82	57.27	48.31	48.26	61.36	55.60	54.62	46.32	47.51	51.39	60.57	59.99
Al2O3	19.44	32.68	32.50	30.97	31.87	29.09	24.90	28.23	26.59	33.00	32.33	23.91	27.51	28.00	33.35	32.95	30.30	24.50	24.20
FeO		0.45	0.49	0.45	0.46	0.58	0.70	0.62	0.57	0.42	0.54	0.79	0.89	0.64	0.45	0.45	0.52	0.73	0.74
CaO		16.75	16.58	14.71	15.70	12.59	7.84	11.46	9.68	16.62	16.47	6.62	10.86	11.45	17.49	17.46	13.72	7.37	7.22
Na2O	11.82	1.93	2.00	3.16	2.58	4.26	6.69	4.77	5.66	1.99	2.11	7.23	5.00	4.81	1.53	1.61	3.60	6.84	6.96
K2O		0.05	0.07	0.12	0.08	0.20	0.73	0.30	0.37	0.08	0.08	1.00	0.32	0.26	0.06	0.05	0.18	0.69	0.77
Total	100.00	100.11	100.01	99.90	100.17	99.83	100.63	100.19	100.14	100.41	99.79	100.90	100.17	99.79	99.21	100.03	99.71	100.70	99.87
Si	3.00	2.21	2.22	2.31	2.26	2.42	2.66	2.48	2.57	2.21	2.22	2.72	2.51	2.48	2.15	2.19	2.35	2.69	2.69
Al	1.00	1.77	1.76	1.67	1.72	1.56	1.31	1.50	1.41	1.78	1.75	1.25	1.46	1.50	1.83	1.79	1.63	1.28	1.28
Fe	0.00	0.02	0.02	0.02	0.02	0.02	0.03	0.02	0.02	0.02	0.02	0.03	0.03	0.02	0.02	0.02	0.02	0.03	0.03
Ca	0.00	0.82	0.82	0.72	0.77	0.61	0.37	0.55	0.47	0.81	0.81	0.31	0.53	0.56	0.87	0.86	0.67	0.35	0.35
Na	1.00	0.17	0.18	0.28	0.23	0.38	0.58	0.42	0.49	0.18	0.19	0.62	0.44	0.42	0.14	0.14	0.32	0.59	0.60
K	0.00	0.00	0.00	0.01	0.00	0.01	0.04	0.02	0.02	0.00	0.00	0.06	0.02	0.01	0.00	0.00	0.01	0.04	0.04
∑ cations	5.00	4.99	4.99	5.00	5.00	5.00	4.99	4.99	4.98	4.99	5.00	4.99	4.99	4.99	5.01	5.00	5.00	4.98	4.99
∑ cations	4.00	3.98	3.98	3.98	3.98	3.98	3.97	3.98	3.98	3.98	3.97	3.97	3.97	3.97	3.98	3.97	3.98	3.97	3.97
∑ cations	1.00	1.00	1.00	1.01	1.00	1.00	0.99	0.99	0.98	0.99	1.00	0.99	0.98	0.99	1.01	1.01	1.00	0.98	1.00
Ab	100.00	17.21	17.85	27.81	22.80	37.52	58.18	42.18	50.31	17.72	18.72	62.61	44.60	42.56	13.63	14.29	31.83	60.18	60.75
An	0.00	82.48	81.72	71.48	76.74	61.33	37.67	56.04	47.52	81.83	80.84	31.69	53.54	55.96	86.03	85.43	67.11	35.83	34.83
Or	0.00	0.31	0.42	0.71	0.46	1.15	4.15	1.78	2.17	0.45	0.44	5.70	1.86	1.49	0.35	0.28	1.06	3.99	4.42

Table A9: Microprobe Data Feldspars analysed in Sample 30 Plagioclase-pyroxene andesite (Plagioclase-pyroxene andesite; Locality: Kiwitahi Tahuna)

Sample	albite-pure	30-area1 plag1	30-area1 plag2	30-area1 plag3	30-area1 plag4	30-area1 plag5	30-area2-plag1	30-area2-plag2	30-area2-plag3	30-area2-plag4	30-area2-plag6	30-area2-plag7-matrix	30-area2-plag8matrix
SiO2	68.74	48.59	49.58	50.18	58.09	56.80	47.10	46.16	48.62	47.40	49.71	55.41	55.45
Al2O3	19.44	32.54	31.82	31.75	26.03	24.94	34.07	33.87	32.19	33.35	31.80	27.09	27.27
FeO		0.47	0.45	0.41	0.87	1.36	0.35	0.34	0.44	0.43	0.49	1.04	0.85
CaO		16.11	15.82	15.31	8.71	8.29	17.46	17.36	15.86	16.88	15.24	10.24	10.13
Na2O	11.82	2.23	2.43	2.70	6.12	6.22	1.56	1.66	2.49	1.94	2.74	5.24	5.13
K2O		0.09	0.12	0.13	0.43	0.44	0.05	0.05	0.09	0.05	0.10	0.38	0.32
Total	100.00	100.03	100.21	100.47	100.26	98.04	100.59	99.44	99.68	100.04	100.09	99.41	99.15
Si	3.00	2.23	2.26	2.28	2.60	2.61	2.15	2.14	2.24	2.18	2.27	2.52	2.52
Al	1.00	1.76	1.71	1.70	1.38	1.35	1.84	1.85	1.74	1.81	1.71	1.45	1.46
Fe	0.00	0.02	0.02	0.02	0.03	0.05	0.01	0.01	0.02	0.02	0.02	0.04	0.03
Ca	0.00	0.79	0.77	0.75	0.42	0.41	0.86	0.86	0.78	0.83	0.75	0.50	0.49
Na	1.00	0.20	0.22	0.24	0.53	0.55	0.14	0.15	0.22	0.17	0.24	0.46	0.45
K	0.00	0.01	0.01	0.01	0.02	0.03	0.00	0.00	0.01	0.00	0.01	0.02	0.02
∑ cations	5.00	5.00	4.99	4.99	4.99	5.00	5.00	5.01	5.01	5.01	5.00	5.00	4.98
∑ cations	4.00	3.98	3.98	3.98	3.98	3.96	3.99	3.99	3.98	3.98	3.98	3.97	3.98
∑ cations	1.00	0.99	1.00	0.99	0.98	0.99	1.00	1.01	1.01	1.01	0.99	0.98	0.97
Ab	100.00	19.91	21.62	24.03	54.58	56.11	13.87	14.72	21.99	17.14	24.40	47.01	46.92
An	0.00	79.58	77.69	75.24	42.89	41.30	85.81	84.99	77.50	82.59	75.02	50.76	51.18
Or	0.00	0.51	0.69	0.73	2.53	2.59	0.32	0.29	0.51	0.27	0.59	2.23	1.90

Table A10: Microprobe Data Feldspars analysed in Sample 38 (Hbl-plag-pyr andesite; Locality: Kiwitahi Miranda)

Sample	albite-pure	38-area2-plag1	38-area2-plag2	38-area2-plag3	38-area2-plag4	38-area2-plag5	38-area3-plag1	38-area3-plag2	38-area3-plag3	38-area3-plag4	38-area4-plag1	38-area4-plag2	38-area4-plag3	38-area4-plag4
SiO2	68.74	55.29	56.36	56.75	57.70	54.29	56.05	52.3	56.7	52.4	55.96	57.05	55.87	52.03
Al2O3	19.44	27.67	27.03	26.38	26.68	28.40	27.21	30.0	26.7	29.3	26.99	26.77	27.53	30.11
FeO		0.37	0.16	0.23	0.20	0.35	0.25	0.3	0.2	0.5	0.22	0.17	0.23	0.48
CaO		10.47	9.76	9.42	9.45	11.47	10.27	13.3	9.7	12.8	9.86	9.68	10.32	13.28
Na2O	11.82	5.06	5.31	5.50	5.85	4.69	5.35	3.7	5.6	3.9	5.53	5.59	5.36	3.67
K2O		0.26	0.24	0.25	0.28	0.23	0.27	0.1	0.3	0.2	0.28	0.29	0.27	0.12
Total	100.00	99.11	98.85	98.52	100.16	99.45	99.40	99.7	99.2	99.1	98.85	99.55	99.56	99.69
Si	3.00	2.51	2.56	2.58	2.58	2.47	2.54	2.4	2.6	2.4	2.54	2.57	2.53	2.37
Al	1.00	1.48	1.44	1.41	1.41	1.52	1.45	1.6	1.4	1.6	1.45	1.42	1.47	1.62
Fe	0.00	0.01	0.01	0.01	0.01	0.01	0.01	0.0	0.0	0.0	0.01	0.01	0.01	0.02
Ca	0.00	0.51	0.47	0.46	0.45	0.56	0.50	0.7	0.5	0.6	0.48	0.47	0.50	0.65
Na	1.00	0.45	0.47	0.48	0.51	0.41	0.47	0.3	0.5	0.3	0.49	0.49	0.47	0.32
K	0.00	0.02	0.01	0.01	0.02	0.01	0.02	0.0	0.0	0.0	0.02	0.02	0.02	0.01
∑ cations	5.00	4.98	4.96	4.96	4.98	4.99	4.98	5.0	5.0	5.0	4.98	4.97	4.98	4.99
∑ cations	4.00	3.99	4.00	4.00	3.99	3.99	3.99	4.0	4.0	4.0	3.99	3.99	3.99	3.99
∑ cations	1.00	0.97	0.95	0.96	0.98	0.99	0.98	1.0	1.0	1.0	0.98	0.97	0.98	0.98
Ab	100.00	45.92	48.89	50.60	51.98	41.97	47.76	32.8	49.9	35.0	49.54	50.22	47.70	33.09
An	0.00	52.51	49.68	47.89	46.38	56.68	50.68	66.3	48.3	63.9	48.78	48.08	50.75	66.18
Or	0.00	1.58	1.44	1.51	1.64	1.35	1.56	0.9	1.8	1.1	1.67	1.70	1.55	0.74

Table A11: Microprobe Data of pyroxenes analysed

Mineral	Diopside	Ferrosilite-	08-area1-px4	19-area1-px1	19-area1-px2	19-area4-opx -3	28-area1-px1	28-area1-px2	28-area3-px	28-area3-px2	28-area4-px1	28-area4-px2
SiO2	55.49	51.73	51.64	52.21	50.93	52.78	53.21	52.06	50.62	52.18	51.29	52.14
Al2O3			2.51	1.35	2.21	0.99	2.84	0.47	3.12	0.43	2.90	1.95
TiO2			0.91	0.26	0.40	0.22	0.20	0.34	0.65	0.34	0.60	0.35
Cr2O3			0.19	0.04	0.01	0.02	0.88	0.07	0.00	0.02	0.02	0.03
FeO		30.93	7.40	19.87	10.11	20.57	5.27	25.11	10.04	24.64	10.16	21.42
MnO			0.21	0.46	0.24	0.52	0.21	0.80	0.27	0.70	0.24	0.46
MgO	18.61	17.35	15.22	23.11	14.37	22.96	17.50	16.97	13.16	16.84	13.43	20.95
CaO	25.90		20.33	1.74	20.00	1.45	20.19	3.65	20.49	3.90	20.02	1.49
Na2O			0.43	0.00	0.32	0.00	0.23	0.06	0.40	0.08	0.33	0.01
Total	100.00	100.00	98.84	99.06	98.60	99.52	100.54	99.53	98.75	99.14	99.00	98.80
Si	2.00	2.00	1.93	1.95	1.93	1.97	1.93	2.00	1.92	2.00	1.93	1.96
Al	0.00	0.00	0.11	0.06	0.10	0.04	0.12	0.02	0.14	0.02	0.13	0.09
Ti	0.00	0.00	0.03	0.01	0.01	0.01	0.01	0.01	0.02	0.01	0.02	0.01
Cr	0.00	0.00	0.01	0.00	0.00	0.00	0.03	0.00	0.00	0.00	0.00	0.00
Fe	0.00	1.00	0.23	0.62	0.32	0.64	0.16	0.81	0.32	0.79	0.32	0.67
Mn	0.00	0.00	0.01	0.01	0.01	0.02	0.01	0.03	0.01	0.02	0.01	0.01
Mg	1.00	1.00	0.85	1.29	0.81	1.27	0.95	0.97	0.74	0.96	0.75	1.18
Ca	1.00	0.00	0.81	0.07	0.81	0.06	0.79	0.15	0.83	0.16	0.81	0.06
Na	0.00	0.00	0.03	0.00	0.02	0.00	0.02	0.00	0.03	0.01	0.02	0.00
∑ cations	4.00	4.00	4.00	4.01	4.02	4.01	4.00	3.98	4.01	3.98	4.00	3.98
∑ cat.	2.00	2.00	2.07	2.06	2.09	2.04	2.07	1.99	2.09	1.97	2.06	2.02
mg-#	100.00	50.00	78.58	67.46	71.69	66.55	85.55	54.65	70.03	54.92	70.19	63.55
Ca/CaFeMnMg	0.50	0.00	0.43	0.04	0.42	0.03	0.41	0.08	0.44	0.08	0.43	0.03
Mg/CaFeMnMg	0.50	0.50	0.45	0.65	0.42	0.64	0.50	0.50	0.39	0.50	0.40	0.61
Fe/CaFeMnMg	0.00	0.50	0.12	0.31	0.16	0.32	0.08	0.41	0.17	0.41	0.17	0.35

APPENDIX B: Detailed petrographic description of samples.

Table B1: petrographic description of samples

Sample Name	Rock Name	Texture	Mineral content	Detailed description of minerals
14-CP-03A	Hornblende-plagioclase Andesite (fresh dyke)	Porphyritic (phenocryst- 55%)	Hornblende (30%), plagioclase (15%), pyroxenes (5%), opaque minerals (5%)	The hornblende is euhedral to subhedral in form and shows glomeroporphyritic texture in some parts of the sample. The hornblende crystals also have opaque rims. The plagioclase is anhedral to subhedral in form. It shows concentric zoning and twinning and most of the crystals have either a deformed or a sieve textured core. Some of the plagioclase cores have inclusions. The opaque minerals are euhedral to subhedral in form
14-CP-04	Plagioclase-pyroxene andesite	Porphyritic (phenocryst- 65%)	Plagioclase (35%), pyroxene (20%), opaque minerals (7%) , olivine (3%),	The plagioclase crystals are euhedral in form with a lath shape, shows twinning and zoning. The pyroxenes are anhedral in form and are mostly altered. The opaque minerals are euhedral to subhedral in form with a hexagonal shape. The olivines are very few and euhedral in form.
14-CP-05	Plagioclase- pyroxene andesite	Porphyritic-aphanitic (Phenocryst-55%)	Plagioclase (30%), pyroxene (10%), Ti-magnetite (5%), Chlorite (5%), Carbonate (3%) Quartz (2%) The matrix is coarse with higher content of lath shaped plagioclase microlites and clinopyroxenes.	Euhedral to subhedral lath-shaped plagioclase crystals. The pyroxenes are euhedral to subhedral and are altered to chlorite in some places . The Ti-magnetite crystals are euhedral to subhedral. The carbonate crystals are evenly spread out thoughtout the sample and mosly with chlorite rims. The quartz crystals are anhedral in shape, sows conchoidal fractures and have chlorite rims.
14-CP-06B	Plagioclase-hornblende Andesite	Vitrophyric (Phenocryst-46%). The phenocryst is set in a black glassy matrix.	Plagioclase (30%), pyroxene (10%) hornblende (6%)	The plagioclase is anhedral to subhedral in form. It shows concentric zoning and twinning. The hornblende is euhedral to subhedral in form

Table B1 (Continued)

Sample Name	Rock Name	Texture	Mineral Content	Detailed description of minerals
14-CP-06D	Plagioclase-hornblende Andesite	Vitrophyric (Phenocryst-60%). The phenocryst is set in a black glassy matrix.	Plagioclase (30%), hornblende (25%), Pyroxene (5%)	The plagioclase is anhedral to subhedral in form. It shows concentric zoning and twinning. Some of the crystals also show cumulophyric texture. The hornblende is euhedral to subhedral in form. It has very thick coronas up to 200 microns thick in places. The hornblende crystals have pyroxene and Ti-magnetite inclusions. The pyroxenes are euhedral to subhedral in form.
14-CP-07	Plagioclase-pyroxene Andesite (Dyke)	Porphyritic (Phenocryst-65%).	Plagioclase (35%), pyroxene (15%), opaque minerals (10%), hornblende (5%)	Euhedral to subhedral plagioclase crystals. It shows concentric zoning and twinning. clinopyoxene inclusions are found in most of them. The pyroxenes are subhedral to anhedral and also exist mostly as part of the groundmass. The hornblende is euhedral to subhedral and is green in colour.
14-CP-08	Basalt	Trachytic (Phenocryst- 45%)	Plagioclase (20%), pyroxene (10%), hornblende (10%), opaque minerals (10%), Olivine (5%)	The plagioclase crystals are euhedral in form and lath-shaped, they show albite twinning and appear to be flowing around the other minerals. The pyroxene crystallites are subhedral in form. The hornblende crystals are euhedral to subhedral with opaque rims. It is seen altering to an opaque mineral in some places. The opaque minerals are relatively the biggest crystals in the sample, measuring up to 1mm. They have inclusions of pyroxenes. The olivines are euhedral to subhedral.
14-CP-10A	Plagioclase-Hornblende Andesite	Porphyritic (Phenocryst- 30%) A micro joint filled with clinopyroxene is also present.	Plagioclase (15%), hornblende (10%), pyroxene (5%)	Euhedral to subhedral plagioclase crystals. Concentric and compos-itionally zoning present with albite twinning. Sieve texture present in the core. Clinopyroxene inclusions are also present in the core and rim. The Hornblende crystals ae euhedral to subhedral in form. The pyroxenes are euhedral to subhedral in form but also occur mainly as inclusions.

Table B1 (Continued)

Sample Name	Rock Name	Texture	Mineral Content	Detailed description of minerals
14-CP-10B	Plagioclase-Hornblende Andesite	Porphyritic (Phenocryst-40%)	Plagioclase (25%), hornblende (10%), pyroxene (5%), Olivine (5%)	Euhedral to subhedral plagioclase crystals. Concentric and compositionally zoning present with albite twinning. The Hornblende crystals are euhedral to subhedral in form. . They are euhedral to subhedral with opaque rims. It is seen altering to an opaque mineral in some places. The pyroxenes are euhedral to subhedral in form. It occur mainly as orthopyroxene. Some have Clinopyroxene lamellae within them. The olivines are very few and euhedral in form.
14-CP-14	Mercury Basalt	Trachytic (Phenocryst-45%)	Plagioclase (30%), pyroxene (10%) Olivine (5%)	Euhedral to subhedral oriented lath shaped plagioclase crystals are present. It is the most dominant mineral and exhibit Carlsbad twinning. The pyroxenes are euhedral to subhedral in form. The olivines are euhedral to subhedral in form.
14-CP-16	Plagioclase-hornblende andesite	Porphyritic aphanitic	Plagioclase (30%), Hornblende (15%), Pyroxene (5%)	Euhedral to subhedral plagioclase crystals. Concentric zoning present with albite twinning. The hornblende crystals are euhedral in form and large in size measuring up to 6mm in length. They are greenish in color with portions of it altered to opaque coloration. They have pyroxene inclusions as well.

Table B1 (Continued)

Sample Name	Rock Name	Texture	Mineral Content	Detailed description of minerals
14-CP-17	Plagioclase- pyroxene andesite	Porphyritic (phenocryst-45%) with intergranular matrix which shows flow pattern in some places.	Plagioclase (25%), pyroxene (15%), olivine (5%), hornblende (5%), opaque minerals (5%)	Euhedral to subhedral plagioclase crystals. Compositional zoning present with albite twinning. Clinopyroxene lamellae is present in most of the crystals. The pyroxene crystals are euhedral to subhedral in form and are large measuring up to 4-5 mm in length. Most of these pyroxenes are orthopyroxenes and have clinopyroxene rims. Olivine is euhedral to subhedral with both large and relatively small crystals. They have cracks with slight alterations along them. The hornblende crystals are euhedral to subhedral in form with opaque rims. The opaque rims have plagioclase inclusions. The opaque minerals are euhedral to subhedral in form.
14-CP-18	Hornblende-pyroxene andesite (lava flow)	Porphyritic aphanitic (phenocryst-50%)	Hornblende (20%), pyroxene (15%), Plagioclase (10%), Biotite (5%), opaque minerals (5%)	The hornblende crystals are euhedral in form and large in size measuring up to 6mm in length. They have cracks with slight alterations along them. Opaque rims and internal opaque spots are also present in them. The pyroxene crystals are euhedral to subhedral in form. The plagioclase crystals are euhedral in form and shows albite twinning and patchy zoning. They also have cracks along them. The Biotite crystals are subhedral in form and have fractures with alteration along them. The opaque minerals are euhedral to subhedral in form.

Table B1 (Continued)

Sample Name	Rock Name	Texture	Mineral Content	Detailed description of minerals
14-CP-19	Hornblende-pyroxene-plagioclase andesite	Porphyritic (phenocryst-40%)	Hornblende (15%), pyroxene (10%), plagioclase (10%), olivine (5%)	The hornblende crystals are euhedral to subhedral in form and have irregular cracks along them. The pyroxenes are euhedral in form with irregular fractures and altered rims. The plagioclase crystals are euhedral to subhedral in form. They show zoning and twinning together with internal embayed spots. Boxy-cellular and sieve textured cores are also present. The olivine crystals are euhedral to subhedral in form.
14-CP-20	Plagioclase-pyroxene andesite.	Porphyritic-aphanitic (phenocryst-45%) The ground mass has visible crystallites of pyroxenes and plagioclases.	Plagioclase (25%), pyroxene (15%), olivine (5%)	The plagioclase crystals are euhedral to subhedral in form. They show zoning and twinning, and most of them are covered up by chlorite (chloritization). The concentric zoning is still showing despite the chloritization. Fractures are present with slight alteration along them. The pyroxenes are euhedral to subhedral and consist of both ortho- and clino-pyroxenes, with the orthopyroxenes being mostly euhedral. Irregular cracks are present throughout the orthopyroxene crystals. The clinopyroxene crystals have inclusions and slightly altered rims. The olivine crystals are euhedral to subhedral in form.
14-CP-22	Hornblende -pyroxene andesite	Porphyritic with dark glassy matrix (vitrophyric) (phenocryst-60%)	Plagioclase (35%), hornblende (10%), pyroxene (10%), opaque minerals (5%)	Plagioclase crystals are euhedral to subhedral and shows twinning and concentric and sector zoning. They also have altered cores, mainly sieve textured. The hornblende crystals are euhedral in form and large measuring up to 3-4mm in length and have thick reaction rims. The coronas have inclusions. The pyroxenes are euhedral to subhedral in form with poorly defined edges. The opaque minerals are euhedral to subhedral in form.

Table B1 (Continued)

Sample Name	Rock Name	Texture	Mineral Content	Detailed description of minerals
14-CP-23	hornblende-pyroxene andesite	Porphyritic with dark glassy matrix (vitrophyric) (phenocryst-60%)	Plagioclase (35%), hornblende (10%), pyroxene (10%), opaque minerals (5%)	Plagioclase crystals are euhedral to subhedral and shows twinning and concentric and sector zoning. They also have altered cores, mainly sieve textured. They also have irregular fractures within them. The hornblende crystals are euhedral in form and have opaque rims. The pyroxenes are euhedral to subhedral in form with poorly defined rims. The opaque minerals are euhedral to subhedral in form.
14-CP-24	Pyroxene-plagioclase andesite	Porphyritic (phenocryst-40%)	Pyroxene (20%), plagioclase (15%), hornblende (5%), opaque minerals (5%)	The pyroxenes are euhedral to subhedral in form and shows concentric zoning and opaque rims. The plagioclase crystals are euhedral to subhedral and shows albite twinning. They also have sieve textured cores and orthopyroxene inclusions in their core. The rims have no inclusions and shows concentric zoning. The hornblende crystals are subhedral in form with opaque rims and internal fractures with alteration along them. The opaque minerals are euhedral to subhedral and evenly spread out throughout the sample.
14-CP-25	Dacite	Trachytic (phenocryst-50%)	Plagioclase (25%), pyroxene (15%), hornblende (5%), biotite (5%), quartz inclusion	The plagioclase crystals are euhedral to subhedral in form and lath shaped. They are aligned in a flow pattern. Carlsbad twinning and oscillatory zoning are present. The pyroxenes are euhedral to subhedral in form, with rims (Back-scattered electron (BSE) images show compositional zoning within the rims). The hornblende crystallites are all subhedral in form. The biotite crystals are all subhedral in form. The quartz inclusion has a round shape and several irregular fractures.

Table B1 (Continued)

Sample Name	Rock Name	Texture	Mineral Content	Detailed description of minerals
14-CP-26	Hornblende-plagioclase andesite	Porphyritic (phenocryst 45%)	Hornblende (20%), plagioclase (15%), pyroxene (5%), Olivine (5%)	The hornblende crystals are euhedral to subhedral in form with opaque rims and internal fractures with alteration along them. The plagioclase crystals are euhedral to subhedral in form. Shows polysynthetic twinning in two directions. Plagioclase with sieve textured core and unaltered rims are present. The sieve texture is also found in the mid portions of some crystals having unaltered core and rim. The pyroxene are euhedral to subhedral in form. They are orthopyroxenes with irregular cracks and have pyroxene inclusions. Most of the orthopyroxenes are mantled by clinopyroxene. Some also have opaque rims. The olivines are euhedral to subhedral in form.
14-CP-28	Plagioclase-pyroxene andesite	Porphyritic trachytic (phenocryst 45%) The groundmass is needle-like and has a flow pattern	Plagioclase (25%), pyroxene (15%), hornblende (5%)	The plagioclase crystals are euhedral to subhedral in form. The crystals have melt inclusions, throughout the sample. They exhibit albite twinning and has pyroxene lamellae running through them. The pyroxenes are euhedral to subhedral in form and have irregular cracks. Some of the pyroxenes have reaction rims. The hornblende crystals are euhedral to subhedral in form. They have irregular cracks and show cleavage.
14-CP-30	Plagioclase-pyroxene andesite	Porphyritic (phenocryst 45%) Fine grained matrix	Plagioclase (25%), Pyroxene (20%)	The plagioclase crystals are euhedral to subhedral in form. Crystals with sieve textured core and smooth rims are present. Albite twinning present and pyroxene lamellae is observed running through some of the plagio-clase crystal. The pyroxenes are euhedral to subhedral in form and have irregular cracks.

Table B1 (Continued)

Sample Name	Rock Name	Texture	Mineral Content	Detailed description of minerals
14-CP-34	Plagioclase- pyroxene-andesite	Subophitic with needle-like matrix (phenocryst 55%)	Plagioclase (35%), pyroxene (15%), opaque minerals (5%)	The plagioclase crystals are euhedral to subhedral in form. The crystals have frozen melt inclusions, throughout the sample. Albite twinning is present as well as sieve textured cores. The pyroxenes are euhedral to subhedral in form. They have inclusions and rims. The opaque minerals are euhedral to subhedral in form.
14-CP-36B	Plagioclase-pyroxene andesite	Porphyritic (phenocryst 45%)	Plagioclase (25%), pyroxene (20%),	The plagioclase crystals are euhedral to subhedral in form. Albite twinning is present as well as sieve textured cores. Some have pyroxene inclusions in the core. There are plagioclase crystals with altered core and smooth rims whereas some crystals also show unaltered core, sieve textured mid-section and smooth unaltered thin rims mantling the alteration surface. The pyroxenes are euhedral to subhedral in form.
14-CP-38	Hornblende-plagioclase-pyroxene andesite	Porphyritic (phenocryst 45%)	Hornblende (20%), plagioclase (20%), pyroxene (15%)	The hornblende crystals are subhedral in in from, with opaque rims. Some of the amphiboles have been altered to iron Ti- magnetite. The plagioclase crystals are euhedral to subhedral in form with a few crystals exhibiting concentric zoning. Some of the crystals have pyroxene inclusions. Few of the crystals have embayed core and smooth rim. Some of the plagioclase crystals also show altered mid-section mantled by thin smooth rims. The pyroxene are euhedral to subhedral in form. They have irregular cracks filled with plagioclase microlite similar to the groundmass plagioclase microlites.